CHALMERS
UNIVERSITY OF TECHNOLOGY

A Physics-Based Distributed-Parameter Equivalent Circuit Model for Lithium-ion Batteries

A physics-based distributed-parameter equivalent circuit model for lithium-ion batteries[☆]

Yang Li[a,*], Mahinda Vilathgamuwa[a], Troy Farrell[b], San Shing Choi[a], Ngoc Tham Tran[a], Joseph Teague[b]

[a] *School of Electrical Engineering and Computer Science, Queensland University of Technology, Brisbane, Queensland, Australia, 4001.*

[b] *School of Mathematical Sciences, Queensland University of Technology, Brisbane, Queensland, Australia, 4001.*

Abstract

A physics-based equivalent circuit model (ECM) is derived by applying the finite volume method to a pseudo-two-dimensional (P2D) model of lithium-ion (Li-ion) batteries. Only standard passive components are used to construct the equivalent circuit, which reflects the fact that a Li-ion battery is an energy storage device. Voltages across and currents through the circuit elements in the ECM are identified with the respective internal electrochemical processes in the battery, thus allowing the parametric values of circuit elements to be expressed as functions of the Li-ion concentrations and temperature. Variations in the parametric values across the thickness of the battery lead to a distributed-parameter ECM amenable for a wide range of applications. Furthermore, in contrast to existing reduced-order models of Li-ion battery which are described by differential-algebraic equations, the ECM is governed by ordinary differential equations wherein all the circuit components are expressed as explicit functions of the state and input variables. Hence, the developed model allows the solution to be found directly using matrix algebra, resulting in rapid simulation study suitable for the development of computationally efficient real-time battery control algorithms. Results of simulation based on the developed distributed-parameter ECM show close agreement with those obtained from a partial differential equation based P2D model under a wide range of applied current rates, but at a much reduced computational burden.

Keywords:

lithium-ion (Li-ion) battery, electrochemical model, finite volume method, equivalent circuit model, battery energy storage system

[☆] Please cite this article as: Y. Li, M. Vilathgamuwa, T. Farrell, S. S. Choi, N. T. Tran, and J. Teague, "A physics-based distributed-parameter equivalent circuit model for lithium-ion batteries," Volume 299 (2019) 451–469, Electrochimica Acta, https://doi.org/10.1016/j.electacta.2018.12.167

[*] Corresponding author

Email address: yangli@ieee.org (Yang Li)

1. Introduction

Due to their relatively high cell voltage, low self-discharge, wide temperature operating range, and an excellent trade-off between power and energy densities, lithium-ion (Li-ion) batteries have become ubiquitous energy storage devices in recent years for use in both mobile applications, including electric vehicles and consumer devices, and stationary applications such as to provide uninterrupted power supply in the form of large-scale, grid-connected, battery energy storage systems (BESS) [1]. As a result of this, advanced battery management systems (ABMS) have been developed using sophisticated physics-based Li-ion battery models that are capable of producing superior battery performance compared to traditional management systems which are based on empirical models [2]. While the empirical models are intuitive and relatively simple to use in control system design and implementation, they do not provide any insights into the internal behaviors of the battery. These internal behaviors furnish important information, such as the internal physical limitation and state of health of these batteries, which needs to be considered for both the short- and long-term battery operations [2]. In contrast, physics-based battery models provide the mathematical description of the electrochemical and thermodynamic processes of the cells [3, 4, 5, 6, 7, 8, 9, 10]. These models are defined by complicated, nonlinear, partial differential algebraic equations (PDAEs) from which the internal behaviors of the battery can be predicted accurately. However, as these PDAEs are not amenable to analytical or computationally efficient numerical solutions, various reduced-order models have been developed, which are either distributed-parameter models [11, 12, 13, 14] or lumped-parameters models [15, 16, 17]. The distributed-parameter models are normally expressed in the form of ordinary differential algebraic equations (DAEs), although to obtain a DAE solver that is computationally efficient and numerically stable for a wide range of battery parameters and operating conditions can still be challenging for real-time applications. The lumped-parameter models are simple and require minimum computational effort. However, they must be fine-tuned according to the electrolyte properties in thick electrodes and/or at high current rates [18].

Another approach to battery modeling is to use equivalent circuit models (ECMs). These have the advantage of ready implementation in well-accepted circuit simulation and control system design software packages such as MATLAB/Simulink [19]. In these packages, various numerical solvers have been incorporated and can be selected to solve the circuit model to facilitate the design of the control system. Conventionally obtained from system identification, the parametric values of such empirical models shall be adjusted regularly to fit the measurement data from tests carried out on-site [20]. However, this approach to battery modeling has limited applicability for long-term battery performance prediction under the ever-changing system dynamics. To address this shortcoming, the ECMs with the capability of describing the internal electrochemical behaviors of Li-ion batteries have been developed in recent years. Based on the single-particle concept, the quantitative linkage between electrochemical models and lumped-parameter ECMs has been studied in [21] and [22], using Pad approximation and polynomial profile approximation techniques, respectively.

Unfortunately the developed models can only be applied to relatively low current rate applications. In [23], the mass and charge transports in the Li-ion battery have been analogized using separate sub-circuits based on the finite difference method (FDM). These sub-circuits have different units and thus cannot be readily implemented in circuit simulation software for the purpose of circuit analysis and control system design. This FDM technique has been used and improved in [24] where an integrated network with the incorporation of double-layer capacitance, thermal behaviors, and the phenomenon of cell degradation is developed. A non-standard circuit component has to be predefined to represent the chemical reactions that occur at various interfaces that govern the conversion between the different species, including electrons, lithium ions and intercalated lithium. The energy and charge conservation is not explicitly exhibited from the perspective of circuit theory. In [25], a semi-empirical multi-particle ECM is developed by considering the non-uniform behaviors along the cell thickness. The transport of lithium ions in the electrolyte is represented by an assumed resistance network with fixed parametric values. The resistance values need to be identified using the electrochemical impedance spectroscopy technique, subject to a large set of experimental data. This method adds complexity to model implementation and it is only verified based on a specific type of Li-ion battery. Similar to the electrochemical models [11, 12, 13, 14], the above-mentioned distributed-parameter ECMs [23, 24, 25] are normally expressed in the form of DAE systems which contain certain algebraic constraints and require a stable and fast DAE solver to ensure accurate results using iterative numerical methods. These DAE solvers can greatly increase the solution time, especially under ever-changing dynamic operating conditions [26]. Also, the degraded performance of the battery under the real-time charging profile has not been evaluated in existing literature where only constant current or pulse current profile are used for model validation. There is no evidence to show these models and the corresponding DAE solution algorithms are sufficiently efficient for use in the context of advanced model-based real-time control schemes operating under realistic fast-dynamic load conditions.

In the current work, a novel computationally efficient physics-based distributed-parameter ECM is developed using finite volume method (FVM). Compared to the existing physics-based ECMs, the ECM presented contains only standard, passive circuit components, a feature that is consistent with the fact that Li-ion batteries are energy storage devices rather than active sources. The conservation of energy of such standard circuit components is well-explained in circuit theory [27]. The use of the standard passive elements means that the model can be analyzed and implemented in readily available circuit simulation software and incorporated battery control schemes in real-time. Each of the components in the ECM presented here is related to a specific, internal, electrochemical process of the Li-ion cell which therefore allows the internal states of the cell to be determined. Furthermore, the proposed ECM is defined by ordinary differential equations (ODEs), without algebraic constraints. Direct solution approaches can therefore be applied and the time-consuming iterative solving procedures for DAEs used in existing literature are avoided. The direct numerical procedure applied here is complemented by taking advantage of the high sparsity of the resulting matrix system [28].

Simulation results obtained based on the developed ECM are shown to agree closely with those produced using the well-established PDAE-based, electrochemical, pseudo-two-dimensional (P2D) model described in [4], but at significantly reduced computational times. Finally, the developed ECM is of a general form that other important cell dynamical processes such as temperature variation [29] and cell degradation that have been well-studied in existing literature can be readily incorporated, while the proposed direct solution method can still be applied.

The rest of the paper is organized as follows. Section 2 proposes a PDAE-based distributed-parameter ECM from the P2D model of Li-ion battery. Section 3 develops the discretized ECM using FVM. The concept of an elementary section (ES) of the equivalent circuit is used. An ES is the basic unit in the ECM and describes the electrochemical behavior in each control volume associated with the discretized ECM model equations. The complete discretized ECM and its solving technique is presented to achieve improved computation efficiency without sacrificing much of the model accuracy. The method to incorporate the impacts of the thermal and side reaction processes is also presented and discussed. Model validation and comparisons are given in Section 4 while the main findings are concluded in Section 5.

2. Electrochemical model of Li-ion battery

2.1. Pseudo-two-dimensional model

A schematic of a 1D-spatial model of the Li-ion cell is shown in Fig. 1. It shows that the cell between the two current collectors has been divided into three domains in the horizontal axis (x-direction), including the positive electrode (denoted by the symbol +), the negative electrode ($-$), and the separator (sep) compartment in-between them. The separator provides electronic insulation but allows ionic conduction. The physical boundaries of the three domains are denoted as $0^+/L^+$, $0^-/L^-$ and $0^{\text{sep}}/L^{\text{sep}}$, respectively. According to the porous-electrode theory and concentrated solution theory, the lattice structure of the electrode can be treated as particles immersed in the electrolyte, and the intercalation process can be modeled by moving lithium ions in or out of the solid particles during charging or discharging. For example, in the charging process as shown in Fig. 1, lithium ions diffuse to the surface of the active material particles (solid phase) within the positive electrode where the electrochemical reaction occurs. Then the lithium ions travel across the separator towards the negative electrode through the electrolyte via diffusion and ionic conduction. Another electrochemical reaction occurs at the particle surface in the negative electrode and lithium ions further diffuse towards the inner regions of the particles until the charging process ends. A similar reverse process occurs when the battery is being discharged. The Li-ion diffusion in the radial direction (r-direction) of the assumed particle exists everywhere along the x-direction, which treats the solid and electrolyte phases as superimposed continua without regard to microstructure/mesostructure [12].

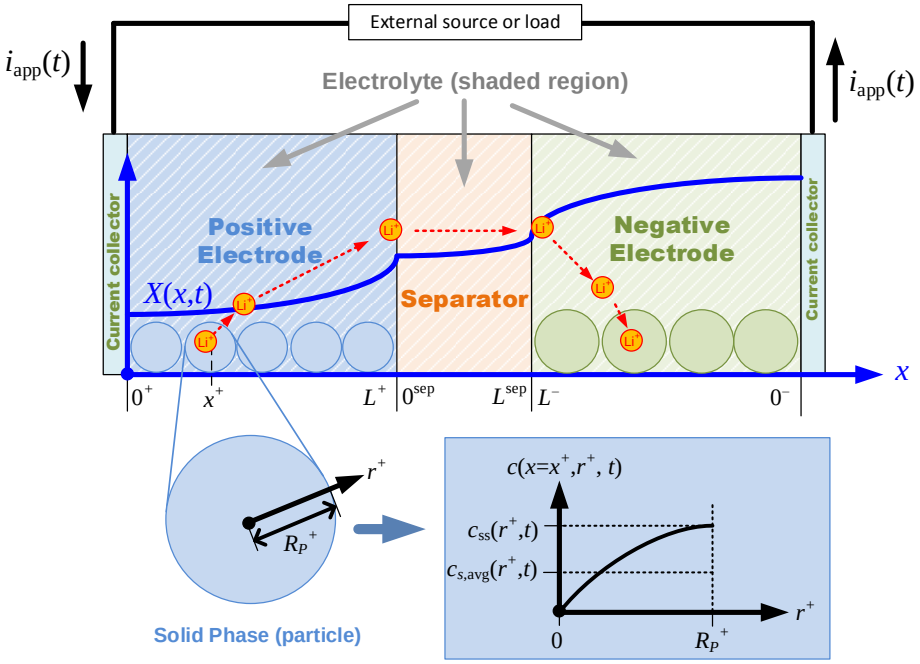

Figure 1: 1D Schematic of P2D model of Li-ion cell during charging. X represents a space- and time-dependent variable.

Such pseudo-2D concept has been adopted to develop various Li-ion cell models with well prediction performance and used in many applications such as [12, 13, 14, 30, 31]. A P2D model of Li-ion cell which consists of a set of coupled, nonlinear PDAEs are presented in Table 1, while the physical meanings of each of the symbols used in the equations are given in the Nomenclature section or explained in [3, 32].

Additional equations of the P2D model pertaining to the parameters U_{ss}, κ, D_e, D_s, and k_0 are given in Appendix A. These parameters are expressed as functions of Li-ion concentrations and temperature, and can be experimentally determined. The detailed expressions may vary based on the materials used for the electrodes and electrolyte. In this article, $LiCoO_2$ and LiC_6 are assumed for the positive and the negative electrodes, respectively, and the expressions are taken from [33].

For example, Equation (10) shows that the equilibrium potential U_{ss} of the electrode is a nonlinear function of the stoichiometry $\theta_{ss} = c_{ss}/c_{s,max}$ at the surface of the assumed particle as well as the temperature T. On the RHS of (10), the first term U^*_{ss} is the equilibrium potential of the electrode at a reference temperature T^* whilst the second term represents the variation of U_{ss} due to temperature change, with the coefficient $\partial U_{ss}/\partial T|_{T^*}$ being the entropic variation of U_{ss}. Both U^*_{ss} and $\partial U_{ss}/\partial T|_{T^*}$ are functions of θ_{ss}, and these relationships are generally denoted by the functions f_s and f_T respectively, given by (A.1)–(A.4).

Next, electrolyte conductivity κ in (1) and electrolyte diffusivity D_e in (5) are functions of the Li-ion concentration c_e in the electrolyte, and the relevant expressions are (A.5) and (A.6).

Table 1: P2D model governing equations

PDEs of P2D Model		Boundary Conditions
Charge conservation in electrolyte phase (domain $= +, -, \text{sep}$)		
$\frac{\partial \Phi_e(x,t)}{\partial x} = -\frac{i_e(x,t)}{\kappa} + \frac{2R_gT(x,t)t_a^0}{F}\frac{\partial \ln c_e(x,t)}{\partial x}$	(1)	$\kappa^{\pm}\frac{\partial \Phi_e}{\partial x}\big\vert_{x=0^{\pm}} = 0,$ $\kappa^{+}\frac{\partial \Phi_e}{\partial x}\big\vert_{x=L^{+}} = \kappa^{\text{sep}}\frac{\partial \Phi_e}{\partial x}\big\vert_{x=0^{\text{sep}}},$ $\kappa^{\text{sep}}\frac{\partial \Phi_e}{\partial x}\big\vert_{x=L^{\text{sep}}} = \kappa^{-}\frac{\partial \Phi_e}{\partial x}\big\vert_{x=L^{-}}$
$\frac{\partial i_e(x,t)}{\partial x} = aFj(x,t) = \frac{3\varepsilon_s}{R_p}Fj(x,t) = J(x,t)$	(2)	$i_e(x,t)\vert_{x=0^{\pm}} = 0,$ $i_e(x,t)\vert_{x=L^{\pm}} = i_e(x,t)\vert_{x\in[0^{\text{sep}},L^{\text{sep}}]} = i_{\text{app}}(t),$ $j(x,t)\vert_{x\in[0^{\text{sep}},L^{\text{sep}}]} = 0$
Charge conservation in solid phase (domain $= +, -$)		
$\frac{\partial \Phi_s(x,t)}{\partial x} = -\frac{i_s(x,t)}{\sigma}$	(3)	$\sigma^{\pm}\frac{\partial \Phi_s}{\partial x}\big\vert_{x=0^{\pm}} = -i_{\text{app}}(t),$ $\sigma^{+}\frac{\partial \Phi_s}{\partial x}\big\vert_{x=L^{+}} = \sigma^{\text{sep}}\frac{\partial \Phi_s}{\partial x}\big\vert_{x=0^{\text{sep}}},$ $\sigma^{\text{sep}}\frac{\partial \Phi_s}{\partial x}\big\vert_{x=L^{\text{sep}}} = \sigma^{-}\frac{\partial \Phi_s}{\partial x}\big\vert_{x=L^{-}}$
$\frac{\partial i_s(x,t)}{\partial x} = -aFj(x,t) = -\frac{3\varepsilon_s}{R_p}Fj(x,t) = -J(x,t)$	(4)	$i_s(x,t)\vert_{x=0^{\pm}} = i_{\text{app}}(t),$ $i_s(x,t)\vert_{x=L^{\pm}} = i_s(x,t)\vert_{x\in[0^{\text{sep}},L^{\text{sep}}]} = 0$
Mass conservation in electrolyte phase (domain $= +, -, \text{sep}$)		
$\frac{\partial c_e(x,t)}{\partial t} = \frac{1}{\varepsilon_e}\frac{\partial}{\partial x}\left(D_e\frac{\partial c_e(x,t)}{\partial x}\right) + \frac{t_a^0}{F\varepsilon_e}\frac{\partial i_e(x,t)}{\partial x}$	(5)	$D_e^{\pm}\frac{\partial c_e}{\partial x}\big\vert_{x=0^{\pm}} = 0,$ $D_e^{+}\frac{\partial c_e}{\partial x}\big\vert_{x=L^{+}} = D_e^{\text{sep}}\frac{\partial c_e}{\partial x}\big\vert_{x=0^{\text{sep}}},$ $D_e^{\text{sep}}\frac{\partial c_e}{\partial x}\big\vert_{x=L^{\text{sep}}} = D_e^{-}\frac{\partial c_e}{\partial x}\big\vert_{x=L^{-}}$
Mass conservation in solid phase (domain $= +, -$)		
$\frac{\partial c_s(x,r,t)}{\partial t} = \frac{1}{r^2}\frac{\partial}{\partial r}\left(D_s r^2\frac{\partial c_s(x,r,t)}{\partial r}\right)$	(6)	$D_s^{\pm}\frac{\partial c_s}{\partial r}\big\vert_{r=0^{\pm}} = 0,$ $D_s^{\pm}\frac{\partial c_s}{\partial r}\big\vert_{r=R_p^{\pm}} = -j(x,t),$ $c_s\vert_{r=R_p^{\pm}} = c_{\text{ss}}^{\pm}(x,t)$
Algebraic Equations in P2D Model		
$j(x,t) = \frac{2i_0(x,t)}{F}\sinh\left(\frac{F\eta_s(x,t)}{2R_gT(x,t)}\right)$	(7)	–
$i_0(x,t) = Fk_0\sqrt{c_e(x,t)(c_{s,\max} - c_{ss}(x,t))c_{ss}(x,t)}$	(8)	–
$\eta_s(x,t) = \Phi_s(x,t) - \Phi_e(x,t) - U_{\text{ss}} - \frac{r_f(x,t)J(x,t)}{a}$	(9)	–
$U_{\text{ss}}(\theta_{\text{ss}},T) = U_{\text{ss}}^* + \frac{\partial U_{\text{ss}}}{\partial T}\big\vert_{T^*}(T(x,t) - T^*)$ $= f_s(\theta_{\text{ss}}) + f_T(\theta_{\text{ss}})(T(x,t) - T^*)$	(10)	–
Output equation of P2D Model		
$V_{\text{bat}}(t) = \Phi_s(0^+,t) - \Phi_s(0^-,t) + (r_{\text{col}}^+ + r_{\text{col}}^-)i_{\text{app}}(t)$	(11)	–

Furthermore, local temperature $T(x,t)$ will also affect κ, D_e, D_s, and k_0. Thermal model of Li-ion cell that governs $T(x,t)$ can be readily incorporated into the presented P2D model (1)–(11) and treated as

a state variable, as will be shown in Section 3.7. In this article, the quantities obtained at the reference temperature will be indicated with a superscript "*".

Note that the presented P2D model provides a generic framework to develop other physics-based Li-ion battery models for the purpose of real-time control. The developed model balances a trade-off between accuracy and computational complexity. The effective properties of the P2D model are assumed known parameters for simulation, and they can be experimentally determined or estimated by using more sophisticated models with the capability to describe the mesostructure of the Li-ion cell [34, 35, 36].

2.2. Approximation of solid phase diffusion equation

PDE (6) is the Fick's law of diffusion equation and it describes the diffusion of lithium ions in the solid phase. The concentration profile in r-direction can be simplified using various techniques [37], among which the polynomial profile approximations establish the relationship between the surface concentration c_{ss}, the volume-averaged concentration $c_{s,\text{avg}}$, the average concentration flux $q_{s,\text{avg}}$ and the ionic flux j [11]. Such approximation methods reduce the order of the P2D model by removing the radial coordinate r, yielding a PDAE model system in x and t, and have been shown to be accurate for various ranges of applied current while satisfying the boundary condition (6) [11]. In this article, (6) will be approximated using a two-parameter polynomial approximation (12), following which the technique to develop the ECM in the following sections will be presented.

$$\begin{aligned} &\tfrac{\partial c_{s,\text{avg}}(x,t)}{\partial t} = -\tfrac{3}{R_p} j(x,t) \\ &\tfrac{5D_s}{R_p}[c_{\text{ss}}(x,t) - c_{s,\text{avg}}(x,t)] = -j(x,t) \end{aligned} \tag{12}$$

Given approximation (12), the governing equations for the variables of the P2D model become (1)–(5) and (7)–(12).

2.3. Model reformulation

The presented approximate P2D model will be reformulated into a distributed-parameter electrical ECM described by PDAEs in this subsection. As (2)–(4) and (11) are already in pure electrical form, only the equations associated with concentration and mass transfer, including (1), (5), (7)–(10), and (12), will be reformulated.

First, Equation (1), which describes electronic conduction in the electrolyte, can be rewritten as

$$\frac{\partial \Phi_e'(x,t)}{\partial x} = -\frac{i_e(x,t)}{\kappa} = \frac{\partial \Phi_e(x,t)}{\partial x} - \frac{\partial V_e(x,t)}{\partial x} \tag{13}$$

Here V_e is a voltage term representing the overpotential due to the diffusion of lithium ions in the electrolyte. Φ_e' is the voltage difference between electrolyte potential Φ_e and V_e. They are defined as

$$V_e(x,t) := \Upsilon T(x,t) \ln[c_e(x,t)/c_e^0] \tag{14}$$

$$\Phi_e'(x,t) := \Phi_e(x,t) - V_e(x,t) \tag{15}$$

where $\Upsilon = 2R_g t_a^0/F$ in (14) is a constant.

Next, following the detailed derivation process in Appendix B.1, the electrolyte diffusion equation (5) can be reformulated to

$$\bar{C}_d \frac{\partial V_e(x,t)}{\partial t} = \frac{\partial}{\partial x}\left(\sigma_d \frac{\partial V_e(x,t)}{\partial x}\right) + J(x,t) \tag{16}$$

Here, $J(x,t)$ is the local volumetric intercalation current density, as presented in (2) and (4). The overbar in (16) and hereafter is used to denote the values that are specified in per unit volume. The volumetric capacitance (in the unit of [F·m^{-3}]) and the conductivity σ_d (in the unit of [S·m^{-1}]) are given as

$$\bar{C}_d = \frac{F\varepsilon_e}{t_a^0}\frac{c_e(x,t)}{\Upsilon T(x,t)}, \qquad \sigma_d = \frac{FD_e(x,t)}{t_a^0}\frac{c_e(x,t)}{\Upsilon T(x,t)} \tag{17}$$

Similarly, following the detailed derivation in Appendix B.2, the equivalent circuit equations for the solid phase diffusion equation (12) and the temperature-dependent equilibrium potential equation (10) are obtained as (18) and (19) respectively:

$$\left.\begin{aligned} &\bar{C}_s^* \tfrac{dV_s^*(x,t)}{dt} = J(x,t) \\ &\bar{G}_1(U_{\rm ss}^*(x,t) - V_s^*(x,t)) = J(x,t) \end{aligned}\right\} \tag{18}$$

$$\left.\begin{aligned} &\bar{C}_{\rm sT} \tfrac{dV_{\rm sT}(x,t)}{dt} = J(x,t) \\ &U_{\rm ss}(x,t) = U_{\rm ss}^*(x,t) + V_{\rm sT}(x,t) \end{aligned}\right\} \tag{19}$$

where the volumetric capacitances and volumetric conductance (in the unit of [F·m^{-3}]) are expressed as

$$\bar{C}_{s,}^* = \frac{F\varepsilon_s c_{s,\max}}{-f_s'(\theta_{s,\rm avg})}, \quad \bar{G}_1 = \frac{F\varepsilon_s c_{s,\max}}{-f_s'(\theta_{s,\rm avg})}\frac{15D_s}{R_P^2}, \quad \bar{C}_{\rm sT} = \frac{1}{T-T^*}\frac{f_s'(\theta_{s,\rm avg})}{f_T'(\theta_{s,\rm avg})}\bar{C}_s^* \tag{20}$$

Note that in (20), f_s' and f_T' represent the derivative functions of f_s and f_T in (10), respectively. Furthermore, the activation overpotential η_s due to the main electrochemical reaction described by the Butler-Volmer equation (7) can be considered to be the voltage across a polarization conductance $\bar{G}_\eta$. Substituting $j = J/(aF)$ into (7) yields the expression of η_s, i.e.,

$$\eta_s(x,t) = \frac{2R_gT(x,t)}{F}\sinh^{-1}\left(\frac{J(x,t)}{2ai_0(x,t)}\right) \tag{21}$$

Dividing local volumetric current density $J(x,t)$ by (21) allows the definition of the conductance $\bar{G}_\eta$:

$$\bar{G}_\eta := \frac{J(x,t)}{\eta_s(x,t)} = \frac{Fai_0}{R_gT(x,t)}\frac{\tau}{\sinh^{-1}(\tau)} \tag{22}$$

where $\tau = J(x,t)/(2ai_0)$, and the exchange current density i_0 is given by (8).

Finally, the volumetric conductance for the solid electrolyte interphase (SEI) film resistance in (9) can be defined as

$$\bar{G}_f := a/r_f \tag{23}$$

With (23) and considering $j = J/(aF)$, Equation (9) becomes

$$\eta_s(x,t) = \Phi_s(x,t) - \Phi_e(x,t) - U_{\rm ss} - J(x,t)/\bar{G}_f \tag{24}$$

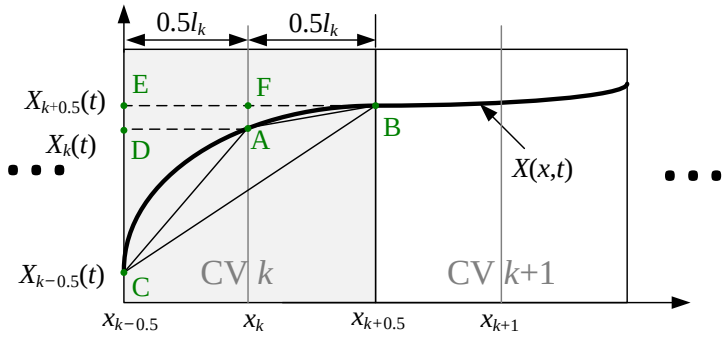

Figure 2: Discretization method.

3. Physics-based ECM of Li-ion battery

3.1. Spatial discretization using finite volume method

For the purposes of computer simulation and model-based control algorithm design, the PDAE-based ECM (2)–(4), (11), (13)–(24) of Li-ion battery needs to be reduced into DAEs so that it can be solved in a real-time environment. This can be achieved by spatial discretization in the x-domain. The FVM is preferred in this article because it is robust, computationally efficient, and capable of preserving the law of mass conservation [38].

In order to correctly carry out the spatial discretization, a mesh structure is first defined by subdividing the x-domain into $N = N^+ + N^{\text{sep}} + N^-$ non-overlapping control volumes (CVs) with geometrically centered nodes. The notation $(N^+, N^{\text{sep}}, N^-)$ will be used to represent the number of CVs. Every CV is associated with a center node x_k and spans the interval $[x_{k-0.5}, x_{k+0.5}]$ as shown in Fig. 2. To facilitate the treatment of boundary and interface conditions, the edges of each CV are aligned with the domain boundaries and internal interfaces. The width of the CV with index k (CV k) is denoted as l_k. Define the central variable $X_k(t) := X(x,t)|x = x_k$, left edge variable $X_{k-0.5}(t) := X(x,t)|x = x_{k-0.5}$, and right edge variable $X_{k+0.5}(t) := X(x,t)|x = x_{k+0.5}$. Also, the following integer sets are defined: $S^+ = \{k : 1 \le k \le N^+\}$, $S^{\text{sep}} = \{k : N^+ + 1 \le k \le N^+ + N^{\text{sep}}\}$, $S^- = \{k : N^+ + N^{\text{sep}} + 1 \le k \le N\}$, and $S = \{k : 1 \le k \le N\}$.

One can use the method of lines [39] to obtain the approximate values of the gradient of the variable $X(x,t)$ at the central node and the edges of CV k. However, this discretization approach requires the use of the values of variables in the neighboring CVs. As shown in Fig. 2, in order to develop an equivalent circuit for each CV for easy model implementation, the discretization equations for method of lines will be modified into the following form, i.e.,

Gradient of central variable:

$$\left.\frac{\partial X(x,t)}{\partial x}\right|_{x=x_k} \approx \frac{X_{k+0.5}(t) - X_{k-0.5}(t)}{l_k} = \frac{|\text{CE}|}{|\text{BE}|} \tag{25}$$

Gradient of left edge variable:

$$\left.\frac{\partial X(x,t)}{\partial x}\right|_{x=x_{k-0.5}} \approx \frac{X_k(t)-X_{k-0.5}(t)}{0.5l_k} = \frac{|\mathrm{CD}|}{|\mathrm{AD}|} \tag{26}$$

Gradient of right edge variable:

$$\left.\frac{\partial X(x,t)}{\partial x}\right|_{x=x_{k+0.5}} \approx \frac{X_{k+0.5}(t)-X_k(t)}{0.5l_k} = \frac{|\mathrm{AF}|}{|\mathrm{BF}|} \tag{27}$$

Based on this method, the spatially-discretized equations for the distributed-parameter ECM are obtained and shown in Table 2. Amongst them, (29)–(33) are obtained by applying (25)–(27) to the PDEs (13), (2)–(4), and (16). The other equations (34)–(37) correspond to (22), (24), (18), and (19), respectively, which only describe the cell behaviors at the central node ($x = x_k$). The units of all the quantities have been converted into [A] (current), [Ω] (resistance), [F] (capacitance). Specifically, $I_{e,k} = Ai_{e,k}$, $I_{s,k} = Ai_{s,k}$, $R_{e,k} = l_k/(\kappa_k A)$, $R_{s,k} = l_k/(\sigma_k A)$, $I_{\mathrm{ionic},k} = Al_k J_k$, $C^*_{s,k} = Al_k \bar{C}^*_{s,k}$, $C_{\mathrm{sT},k} = Al_k \bar{C}_{\mathrm{sT},k}$, $C_{d,k} = Al_k \bar{C}_{d,k}$, $R_{f,k} = 1/(Al_k \bar{G}_{f,k})$, $R_{1,k} = 1/(Al_k \bar{G}_{1,k})$, $R_{\eta,k} = 1/(Al_k \bar{G}_{\eta,k})$. Special attention has to be paid to the resistance $R_{d,k,k+0.5}$ and $R_{d,k,k-0.5}$ in (33). They are expressed as

$$R_{d,k,k\pm0.5} = \frac{0.5l_k}{A\sigma_{d,k\pm0.5}} = \frac{0.5l_k}{A}\left(\frac{t^0_a}{FD_{e,k\pm0.5}}\frac{\Upsilon T_{k\pm0.5}}{c_{e,k\pm0.5}}\right) \approx \frac{0.5\Upsilon t^0_a}{AF}\frac{l_k T_k}{D_{e,k}}\frac{\partial \ln c_{e,k\pm0.5}}{\partial c_{e,k\pm0.5}} \tag{28}$$

Note that in the separator, as there is no ionic flux j, the term $I_{\mathrm{ionic},k}$ in (30) and (33) shall be set to zero when it is applied to a CV in the separator domain.

Taken together, the FVM ECM equations describe the dynamic behavior of the CV k in the cell.

3.2. Elementary section

With the spatially-discretized ECM equations derived in Section 3.1, the equivalent circuit of each CV, denoted the elementary section (ES), will be developed. First, the equivalent circuit to (29)–(32) and (35), which shows the principle of charge and energy conservation, is obtained according to Kirchhoffs circuit laws and is shown in Fig. 3(a). This circuit describes electronic and ionic conduction processes in a CV and it is referred to as an ES of the main circuit. Note that Fig. 3(a) is only valid for a CV in the electrode domain ($k \in S^+ \cup S^-$). It is reduced to Fig. 3(b) for a CV in the separator domain ($k \in S^{\mathrm{sep}}$), taking into account the fact that there is no ionic flux (i.e., $I_{\mathrm{ionic},k} = j_k = 0$) in the separator.

Consider the controlled voltage source (CVS) of the equilibrium potential $U_{\mathrm{ss},k}$ in Fig. 3(a). It is associated with the diffusion of lithium ions in the solid phase governed by (36) and (37). According to (36) and (37), the equivalent circuit associated with $U_{\mathrm{ss},k}$ is obtained and it is shown in Fig. 3(g). It can be seen that $U_{\mathrm{ss},k}$ consists of three components:

1) $V^*_{s,k}$ represents the open-circuit potential (OCP) of the electrode at reference temperature T^*;

2) $V_{\mathrm{sT},k}$ represents the variation of OCP due to the temperature change;

Table 2: FVM ECM equations

FVM ECM Equations	Boundary Conditions
$\Phi_{e,k\pm0.5}(t) - \Phi'_{e,k}(t) = \mp 0.5 R_{e,k} I_{e,k\pm0.5}(t) + V_{e,k\pm0.5}(t)$ (29)	$\Phi_{e,0.5} = \Phi'_{e,1}$, $\Phi'_{e,N} = \Phi_{e,N+0.5}$
$I_{e,k+0.5}(t) - I_{e,k-0.5}(t) = I_{\text{ionic},k}(t)$ (30)	$I_{e,0.5} = I_{e,N+0.5} = 0$, $I_{e,N^+ +0.5} = I_{e,N^+ + N^{\text{sep}}+0.5} = I_{e,k}\vert_{k\in S^{\text{sep}}} = I_{\text{app}}$
$\Phi_{s,k}(t) - \Phi_{s,k\pm0.5}(t) = \pm 0.5 R_{s,k} I_{s,k\pm0.5}(t)$ (31)	$\Phi_{s,N^+} = \Phi_{s,N^+ +0.5}$, $\Phi_{s,N^-} = \Phi_{s,N^- -0.5}$
$I_{s,k+0.5}(t) - I_{s,k-0.5}(t) = -I_{\text{ionic},k}(t)$ (32)	$I_{s,0.5} = I_{s,N+0.5} = I_{\text{app}}$, $I_{s,N^+ +0.5} = I_{s,N^+ + N^{\text{sep}}+0.5} = I_{s,k}\vert_{k\in S^{\text{sep}}} = 0$
$C_{d,k} \frac{dV_{e,k}(t)}{dt} = \frac{V_{e,k+0.5}(t) - V_{e,k}(t)}{R_{d,k,k+0.5}} - \frac{V_{e,k}(t) - V_{e,k-0.5}(t)}{R_{d,k,k-0.5}} + I_{\text{ionic},k}(t)$ (33)	$V_{e,0.5} = V_{e,1}$, $V_{e,N} = V_{e,N+0.5}$
$\eta_{s,k}(t) = R_{\eta,k} I_{\text{ionic},k}(t)$ (34)	-
$\Phi_{s,k}(t) - \Phi_{e,k}(t) = U_{\text{ss},k} + \eta_{s,k}(t) + R_{f,k} I_{\text{ionic},k}(t)$ (35)	-
$C^*_{s,k} \frac{dV^*_{s,k}(t)}{dt} = I_{\text{ionic},k}(t), \quad U^*_{\text{ss},k}(t) - V^*_{s,k}(t) = R_{1,k} I_{\text{ionic},k}(t)$ (36)	-
$C_{sT,k} \frac{dV_{\text{sT},k}(x,t)}{dt} = I_{\text{ionic},k}(t), \quad U_{\text{ss},k}(t) = U^*_{\text{ss},k}(t) + V_{\text{sT},k}(t)$ (37)	-

3) $\Delta U_k = U^*_{\text{ss},k} - V^*_{s,k} = R_{1,k} I_{\text{ionic},k}$ represents the overpotential due to the diffusion of lithium ions in the solid phase.

As mentioned earlier in Section 2.2, there are many methods to approximate (6), instead of the two-parameter polynomial approximation method adopted here. Different methods can result in different RC equivalents to CVS U_{ss}. As another example, Appendix B.2 gives the derivation of RC equivalence using a higher-order polynomial approximation which is more accurate for higher current application [11], and its equivalent circuit is shown in Fig. 3(h). The study on the other methods of approximation has been left for future work and is expected to bring fruitful outcomes.

Fig. 3(c) shows the electrical circuit for (33), which describes the mass transfer in the electrolyte in the electrode domain. It is denoted the ES of the supplementary circuit. Again, for the separator domain ($k \in S^{\text{sep}}$), as $I_{\text{ionic},k} = 0$, the corresponding ES can be reduced to Fig. 3(d). Next, it can be seen that the CVS $V_{e,k}$ in Fig. 3(a) and the controlled current source (CCS) $I_{\text{ionic},k}$ in Fig. 3(c) are coupled components and they constitute a lossless two-port network component, as shown in Fig. 3(e). This component represents an ideal transformer with turns ratio of 1:1, as shown in Fig. 3(f). As the two terminals have equal terminal powers $V_{e,k} I_{\text{ionic},k}$, this ideal transformer component clearly embodies the principle of conservation of energy

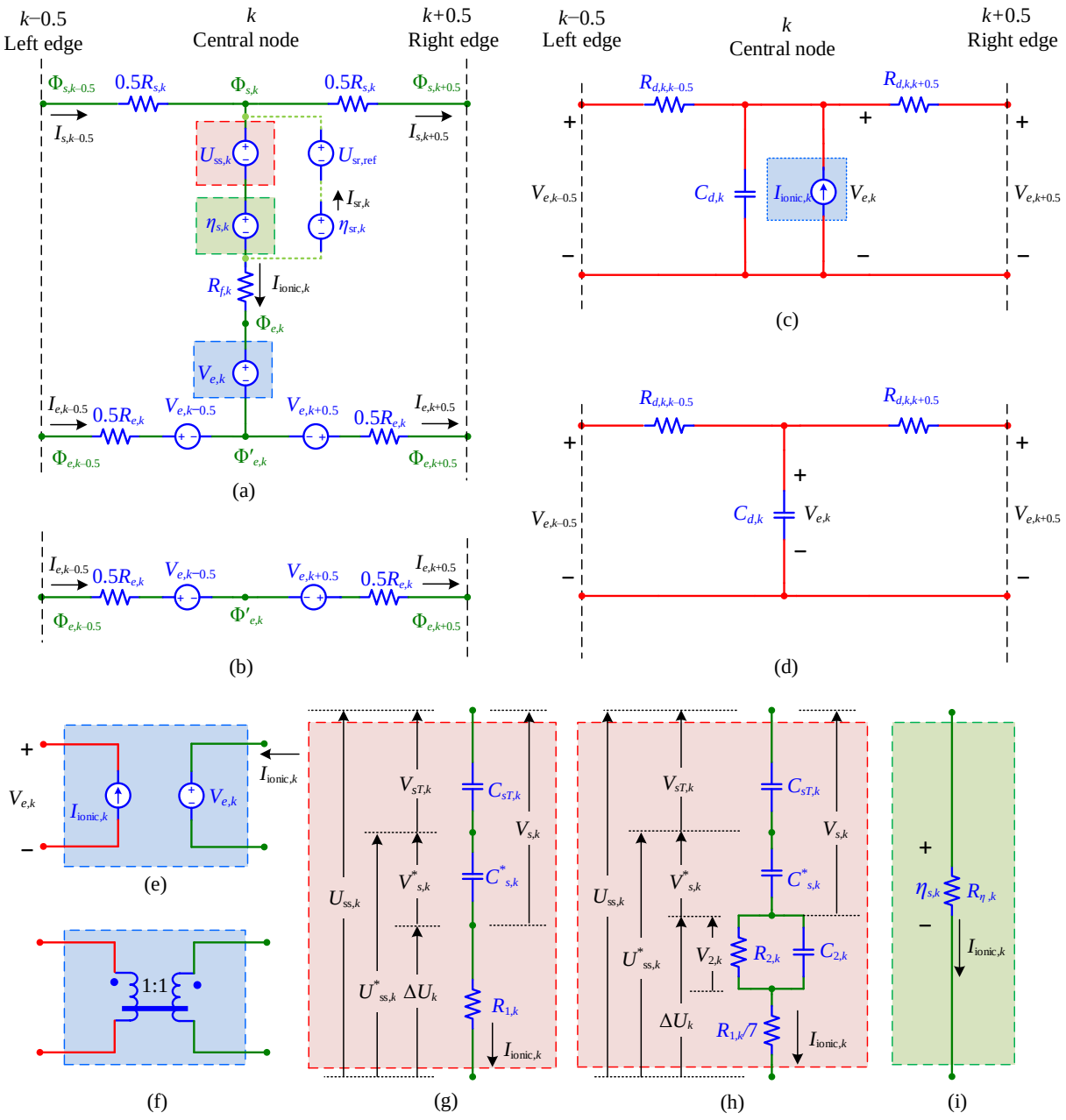

Figure 3: (a) ES of the main circuit of the electrode; (b) ES of the main circuit of the separator; (c) ES of the supplementary circuit of the electrode; (d) ES of the supplementary circuit of the separator. (e) Coupled CCS and CVS; (f) Ideal transformer equivalence of coupled CCS and CVS. (g) RC equivalence to equilibrium potential $U_{\mathrm{ss},k}$ using two-parameter polynomial approximation; (h) RC equivalence to equilibrium potential $U_{\mathrm{ss},k}$ using higher-order polynomial approximation; (i) R equivalence to main reaction overpotential $\eta_{s,k}$.

between the charge transfer (main circuit) and mass transfer (supplementary circuit) processes. This feature has not been explicitly exhibited in existing literature from the perspective of circuit theory.

3.3. Construction of the full ECM

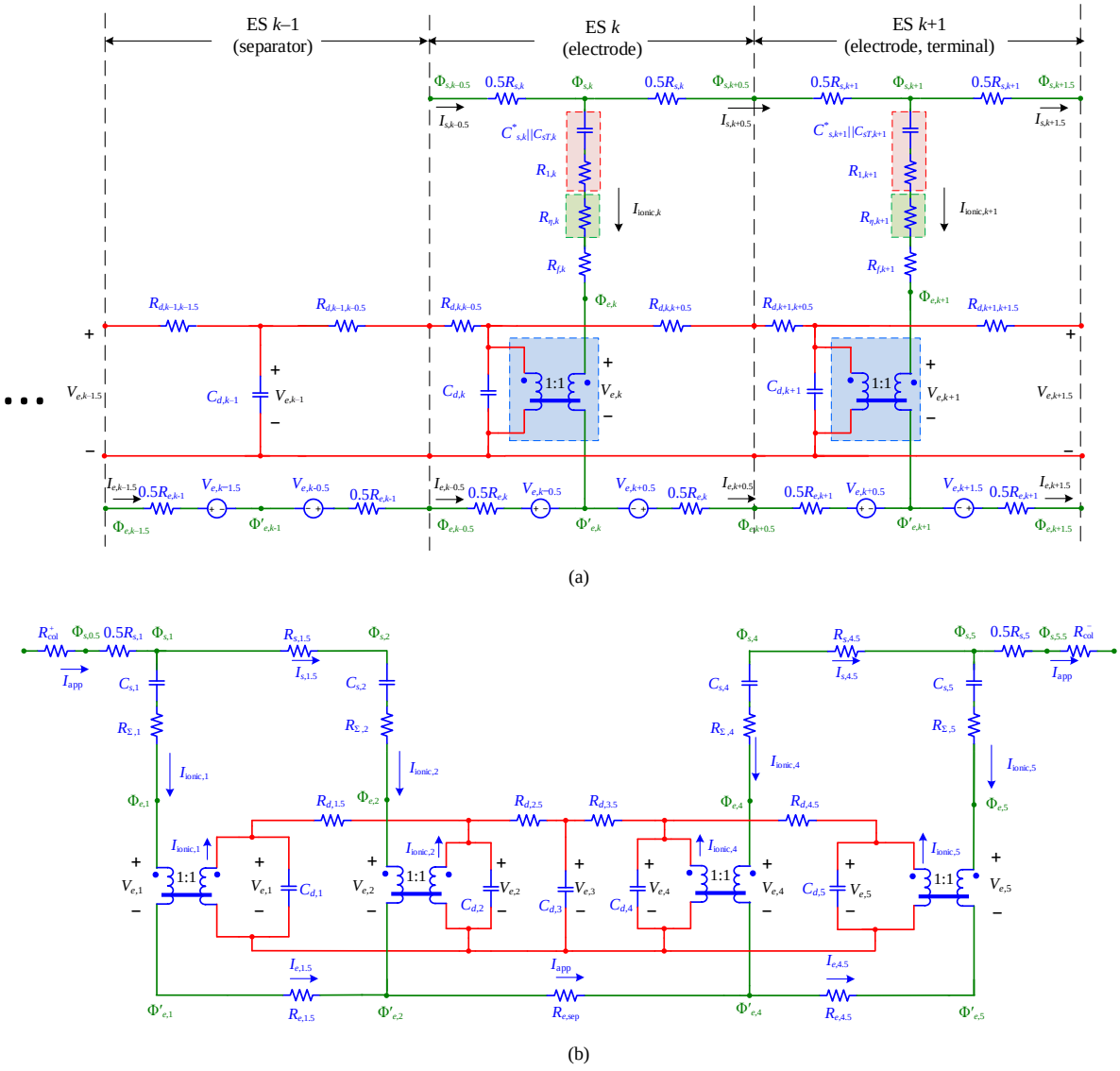

Figure 4: (a) Three ESs connected in series; (b) Simplified equivalent circuit for $(N^+, N^{\text{sep}}, N^-) = (2, 1, 2)$. Note that $R^{\pm}_{\text{col}} = r^{\pm}_{\text{col}}/A$.

According to FVM, the right edge variable of CV k is identical to the left edge variable of CV $k+1$. This requirement of continuity can be automatically satisfied by cascading different ESs. As an example, Fig. 4(a) shows part of the circuit consisting of three cascaded ESs: ES $k-1$ and ES k are at the interface of the separator and the negative electrode, while ES $k+1$ is at the end terminal of the electrode.

After cascading, it is possible to simplify the ECM by reducing the number of circuit components. Firstly, the capacitors and resistors connected in series can be combined:

With this combination, the ODEs that govern the capacitor voltages are changed from (36), (37), and (33) to

$$C_{s,k}\frac{dV_{s,k}(t)}{dt} = I_{\text{ionic},k}(t) \tag{38}$$

$$C_{d,k}\frac{dV_{e,k}(t)}{dt} = \frac{V_{e,k+1}(t) - V_{e,k}(t)}{R_{d,k+0.5}} + \frac{V_{e,k-1}(t) - V_{e,k}(t)}{R_{d,k-0.5}} + I_{\text{ionic},k}(t) \tag{39}$$

In (38), the capacitor voltage $V_{s,k} = V^*_{s,k} + V_{\text{sT},k}$ represents the temperature-dependent OCP as indicated in Fig. 3(g). Secondly, certain floating branches can be deleted if no current flows into them. This can be investigated from the boundary conditions. For example, according to boundary conditions of (32), $I_{e,k+1.5} = 0$ and $I_{s,k-0.5} = 0$. Thus, the bottom-right branch of the ES $k+1$ and the top-left branch of ES k of the main circuit can be removed. Similarly, according to boundary conditions of (33) $V_{e,k+1} = V_{e,k+1.5}$, the extra branches on the right-hand side terminal of the supplementary circuit can also be deleted. Thirdly, the two series-connected CVSs on the same branches at the bottom of the main circuit effectively cancel each other out, as the pair have equal but opposite polarities. As an example, Fig. 4(b) shows the complete equivalent circuit of Li-ion battery for $(N^+, N^{\text{sep}}, N^-) = (2, 1, 2)$ by applying the above circuit simplification steps.

3.4. State-space representation of physics-based ECM

The complete distributed-parameter ECM of Li-ion battery cell denoted DAE-OCM has now been derived. It can be observed that only standard passive circuit components consisting of resistors, capacitors, and ideal transformers are used to form the circuit. Hence, according to conventional circuit theory, the ECM can now be readily expressed in a compact state-space form, namely,

$$\left.\begin{aligned} \tfrac{d}{dt}\mathbf{x}_c(t) &= \mathbf{A}_c\mathbf{x}_c(t) + \mathbf{B}_c u(t) \\ y(t) &= \mathbf{C}_c\mathbf{x}_c(t) + \mathbf{D}_c u(t) \end{aligned}\right\} \tag{40}$$

Here, the input variable $u(t)$ is the applied current $I_{\text{app}}(t) = Ai_{\text{app}}(t)$, the output variable $y(t)$ is the terminal voltage $V_{\text{bat}}(t)$, and the state vector $\mathbf{x}_c(t)$ consists of all the capacitor voltages in the ECM, viz.,

$$\mathbf{x}_c(t) = \begin{bmatrix} \mathbf{V}_s^+(t) \\ \mathbf{V}_s^-(t) \\ \mathbf{V}_e^+(t) \\ \mathbf{V}_e^{\text{sep}}(t) \\ \mathbf{V}_e^-(t) \end{bmatrix}$$

where

$$\mathbf{V}_s^+ = \begin{bmatrix} V_{s,1} \\ V_{s,2} \\ \vdots \\ V_{s,N^+-1} \\ V_{s,N^+} \end{bmatrix}, \mathbf{V}_s^- = \begin{bmatrix} V_{s,N^+ + N^{\text{sep}}+1} \\ V_{s,N^+ + N^{\text{sep}}+2} \\ \vdots \\ V_{s,N-1} \\ V_{s,N} \end{bmatrix}$$

$$\mathbf{V}_e^+ = \begin{bmatrix} V_{e,1} \\ V_{e,2} \\ \vdots \\ V_{e,N^+-1} \\ V_{e,N^+} \end{bmatrix}, \mathbf{V}_e^{\text{sep}} = \begin{bmatrix} V_{e,N^+ +1} \\ V_{e,N^+ +2} \\ \vdots \\ V_{e,N^+ + N^{\text{sep}}-1} \\ V_{e,N^+ + N^{\text{sep}}} \end{bmatrix}, \mathbf{V}_e^- = \begin{bmatrix} V_{e,N^+ + N^{\text{sep}}+1} \\ V_{e,N^+ + N^{\text{sep}}+2} \\ \vdots \\ V_{e,N-1} \\ V_{e,N} \end{bmatrix}$$

The equations in (40) represent a continuous-time single-input single-output (SISO) state-space model. The elements in the matrices $\mathbf{A}_c$, $\mathbf{B}_c$, $\mathbf{C}_c$, and $\mathbf{D}_c$ are functions of the RC parameters and the detailed derivation of them are given in Appendix C.

3.5. ODE-ECM

For implementation as a real-time control system, (40) has to be discretized in time and solved numerically. In order to perform the numerical integration to obtain the state vector $\mathbf{x}_c(t + \Delta t)$ at the next time step, the values of $\mathbf{A}_c$, $\mathbf{B}_c$, $\mathbf{C}_c$, and $\mathbf{D}_c$ must be updated within each time step Δt. The RC parameters that determine $\mathbf{A}_c$, $\mathbf{B}_c$, $\mathbf{C}_c$, and $\mathbf{D}_c$, according to (17), (20), (22), and (23), depend on the following variables: $c_{e,k}(t)$, $\theta_{s,\text{avg},k}(t)$, $\theta_{\text{ss},k}(t)$, and $\tau_k(t)$ (which is proportional to $I_{\text{ionic},k}(t)$). Amongst them, $c_{e,k}(t)$ and $\theta_{s,\text{avg},k}(t)$ can be directly calculated from the state variables $\mathbf{x}_c(t)$ using (14) and (B.4), respectively. To obtain the remaining two variables $\theta_{\text{ss},k}(t)$ and $I_{\text{ionic},k}(t)$, a highly nonlinear algebraic equation system has to be solved:

$$0 = g(\mathbf{I}_{\text{ionic}}(t), \boldsymbol{\theta}_{\text{ss}}(t), u(t)) \tag{41}$$

where $\mathbf{I}_{\text{ionic}}(t)$ and $\boldsymbol{\theta}_{\text{ss}}(t)$ are vectors of $I_{\text{ionic},k}(t)$ and $\theta_{\text{ss},k}(t)$, respectively. Together, (40) and (41) represent a system of DAEs that govern the differential variables $\mathbf{x}_c(t)$ and the algebraic variables $\mathbf{I}_{\text{ionic}}(t)$ and $\boldsymbol{\theta}_{\text{ss}}(t)$ for the DAE-ECM. This algebraic equation imposes an implicit algebraic constraint to the model (40). Due to the fact that (41) is highly nonlinear, an iterative method must be used within each time step Δt to calculate the value of $\mathbf{I}_{\text{ionic}}(t)$ and $\boldsymbol{\theta}_{\text{ss}}(t)$with known $u(t) = I_{\text{app}}(t)$. Such a process would increase the solution time significantly and may even lead to numerical instability, especially in situations where the input current, $I_{\text{app}}(t)$, varies dramatically [40]. In fact, $\theta_{\text{ss},k}(t)$, $I_{\text{ionic},k}(t)$ are only used in (22). In order to remove the constraint (41) of the DAE-based model, an approach is now proposed to approximate $I_{\text{ionic},k}(t)$ and $\theta_{\text{ss},k}(t)$ so that (22) can be expressed as a function of state and input variables.

First, the profile of ionic flux $j(x,t)$ in the x-direction will be estimated by a quadratic function for each electrode. For the positive electrode, assuming the gradient of j at $x = 0$ is zero, the estimated ionic flux is expressed as

$$\hat{j}(x,t) = \gamma^{+} x^2 \tag{42}$$

A "ˆ" symbol will be used to denote the estimated quantities. Integrating (4) from 0^+ to L^+ gives

$$\int_{0^+}^{L^+} -a^{+} F \hat{j}(x,t) dx^{\pm} = \int_{0^+}^{L^+} \frac{\partial i_s(x,t)}{\partial x} dx = i_s(x,t)|_{x=L^+} - i_s(x,t)|_{x=0^+} = -i_{\text{app}}(t) \tag{43}$$

Substituting (42) into (43) yields

$$\gamma^{+} = \frac{3}{a^{+} F (L^{+})^3} i_{\text{app}}(t) \tag{44}$$

The relationship between central node index k and spatial position x is

$$x = \frac{2k-1}{2N^{+}} L^{+} \tag{45}$$

Substituting (44) and (45) into (42), and using $I_{\text{ionic},k} = A l_k a_k F j_k = A(L^{+}/N^{+}) a_k F j_k$, the relationship between $\hat{I}_{\text{ionic},k}$ and I_{app} is obtained:

$$\hat{I}_{\text{ionic},k}(t) = \frac{3}{N^{+}} \left(\frac{2k-1}{2N^{+}} \right)^2 I_{\text{app}}(t) \tag{46}$$

A similar approach can be applied to the negative electrode, which yields

$$\hat{I}_{\text{ionic},k}(t) = -\frac{3}{N^{-}} \left(\frac{4N - 2N^{-} - 2k + 1}{2N^{-}} \right)^2 I_{\text{app}}(t) \tag{47}$$

Next, considering (36), the surface stoichiometry $\theta_{\text{ss},k}(t)$ can be estimated using

$$\hat{\theta}_{\text{ss},k}(t) = f_s^{-1}(\hat{U}^{*}_{\text{ss},k}(t)) = f_s^{-1}(V^{*}_{s,k}(t) + R_{1,k} \hat{I}_{\text{ionic},k}(t)) \tag{48}$$

Hence, using (47) and (48), (22) can be estimated based on input variable $I_{\text{app}}(t)$ and state variable $V^{*}_{s,k}(t)$, and the resulting model is denoted as ODE-ECM. Table 3 summarizes the expressions that determine the R and C parametric values of the ODE-ECM. All the RC parameters as well as the matrices $\mathbf{A}_c$, $\mathbf{B}_c$, $\mathbf{C}_c$, and $\mathbf{D}_c$ have been expressed as explicit functions of the state variables $\mathbf{x}_c(t)$ and input variable $I_{\text{app}}(t)$, and thus the derivative of the state variables can be rapidly calculated without using an iterative method. The physical meaning of each component and their dependence on state and input variables are also shown in Table 3.

Note that in obtaining the expression of $R_{d,k+0.5}$, the following approximation is used:

$$\frac{\partial \ln c_{e,k+0.5}}{\partial c_{e,k+0.5}} \approx \frac{\ln c_{e,k+1} - \ln c_{e,k}}{c_{e,k+1} - c_{e,k}} = \frac{1}{c_{e,k}} \frac{\ln(c_{e,k+1}/c_{e,k})}{c_{e,k+1}/c_{e,k} - 1} = \frac{1}{c_{e,k}} \frac{\chi_{k+1,k}}{\exp(\chi_{k+1,k}) - 1} \tag{49}$$

where

$$\chi_{k+1,k} := \ln(c_{e,k+1}/c_{e,k}) = \frac{V_{e,k+1}}{\Upsilon T_{k+1}} - \frac{V_{e,k}}{\Upsilon T_k} \tag{50}$$

Table 3: Expressions and physical meanings of circuit components of ODE-ECM

Sym.	Expressions	Physical Meanings	Dependent state and input variables
$C_{s,k}$	$\left(\frac{1}{1+\frac{f_T(\theta_{s,\text{avg},k})}{f_s(\theta_{s,\text{avg},k})}(T_k-T^*)}\right)\times$ $\frac{Al_kF\varepsilon_{s,k}c_{s,\max,k}}{-f_s'(\theta_{s,\text{avg},k})}$	Capacitance due to the transport of lithium ions in the solid phase with temperature effect	$V_{s,k}(\theta_{s,\text{avg},k})$
$R_{1,k}$	$\frac{-f_s'(\theta_{s,\text{avg},k})}{Al_kF\varepsilon_{s,k}c_{s,\max,k}}\frac{R_{p,k}^2}{15D_{s,k}}$	Local virtual resistance representing the dissipation due to Li-ion diffusion in solid phase	$V_{s,k}(\theta_{s,\text{avg},k})$
$R_{s,k+0.5}$	$\frac{0.5}{A}\left(\frac{l_k}{\sigma_k}+\frac{l_{k+1}}{\sigma_{k+1}}\right)$	Local resistance in solid phase	None
$R_{e,k+0.5}$	$\frac{0.5}{A}\left(\frac{l_k}{\kappa_k}+\frac{l_{k+1}}{\kappa_{k+1}}\right)$	Local resistance in the electrolyte	$V_{e,k}(c_{e,k})$, $V_{e,k+1}(c_{e,k+1})$
$R_{d,k+0.5}$	$\frac{0.5\Upsilon t_a^0}{AF}\left(\frac{l_kT_k}{D_{e,k}}+\frac{l_{k+1}T_{k+1}}{D_{e,k+1}}\right)\times$ $\frac{1}{c_{e,k}}\frac{\chi_{k+1,k}}{\exp(\chi_{k+1,k})-1}$	Local virtual resistance representing the dissipation due to Li-ion diffusion in the electrolyte	$V_{e,k}(c_{e,k})$, $V_{e,k+1}(c_{e,k+1})$
$C_{d,k}$	$\frac{Al_kF\varepsilon_{e,k}c_{e,k}}{t_a^0\Upsilon T_k}$	Capacitance due to the concentration in the electrolyte	$V_{e,k}(c_{e,k})$
$R_{\eta,k}$	$\frac{1}{Al_ka_k}\frac{R_gT_k}{F^2k_{0,k}c_{s,\max,k}}\times$ $\frac{1}{\sqrt{c_{e,k}\hat{\theta}_{\text{ss},k}(1-\hat{\theta}_{\text{ss},k})}}\frac{\sinh^{-1}(\hat{\tau}_k)}{\hat{\tau}_k}$	Local resistance due to the main reaction	$V_{e,k}(c_{e,k})$, $V_{s,k}(\theta_{s,\text{avg},k})$, I_{app}
$R_{f,k}$	$\frac{r_{f,k}}{Al_ka_k}$	Local SEI film resistance	None

As (49) has a removable discontinuity at $\chi_{k+1,k}=0$, one can redefine its value by recognizing that

$$\lim_{\chi_{k+1,k}\to 0}\frac{\chi_{k+1,k}}{\exp(\chi_{k+1,k})-1}=1 \tag{51}$$

One can use the steady-state values, when $I_{\text{app}}(0)=0$, to initiate the time-domain simulation. At steady state, initial $V_{e,k}(0)=0$, and the initial values of $V_{s,k}^*$ can be calculated using the initial state-of-charge (SOC) and T. The SOC at node k is defined here as the portion of total stored charge in the main capacitor $V_{s,k}^*$. As the volume-averaged concentration $\theta_{s,\text{avg}}$ is proportional to the charges stored in the main capacitor, one obtains

$$\text{SOC}_k(t)=\begin{cases}1-\frac{\theta_{s,\text{avg},k}(t)-\theta_{0\%}^+}{\theta_{100\%}^+-\theta_{0\%}^+}=1-\frac{f_s^+(V_{s,k}^*(t))-\theta_{0\%}^+}{\theta_{s,100\%}^+-\theta_{0\%}^+}, & k\in S^+\\ \frac{\theta_{s,\text{avg},k}(t)-\theta_{0\%}^-}{\theta_{100\%}^--\theta_{0\%}^-}=\frac{f_s^-(V_{s,k}^*(t))-\theta_{0\%}^-}{\theta_{100\%}^--\theta_{0\%}^-}, & k\in S^-\end{cases} \tag{52}$$

where $\theta_{100\%}^+$ and $\theta_{0\%}^+$ are the corresponding stoichiometry for the fully-charged and the fully-discharged positive electrode, and $\theta_{100\%}^-$ and $\theta_{0\%}^-$ have similar meanings for the negative electrode. Next, the ODE-

ECM can be discretized in the time domain and solved by various well-established numerical methods for the purposes of computer simulation and real-time control. The system order of the ECMs equals to the number of the capacitors: this is $2N^+ + 2N^- + N^{\text{sep}}$ if the two-parameter Li-ion concentration approximation model is used to represent the transport process of the Li-ion in the solid phase. As can also be seen in Appendix C, the matrices of the state-space model of the developed ECM are sparse. Well-established numerical methods for dealing with sparse matrices can be used to reduce solution time [29].

It should be pointed out that when $(N^+, N^{\text{sep}}, N^-) = (1, 0, 1)$, the resulting ECM represents the single-particle model (SPM), which is a lumped-parameter model relevant in low current rate applications. This ECM for SPM has been reported in [22]]. When $(N^+, N^{\text{sep}}, N^-) = (1, 1, 1)$, the ECM represents the equivalent circuit for an extended single-particle model, as proposed in [41] where diffusion of Li-ion in the electrolyte is considered. These models are valid for low current rate applications where the distributed effect of variables along the cell thickness is ignored.

3.6. Conservation of mass

One important feature of the developed ECM is that the law of mass conservation is preserved. This can be proven in the following way. The mass of the lithium ions in the CV k in the solid phase can be calculated using the concentration, $c_{s,k}(t)$, and the effective volume, $Al_k\varepsilon_{s,k}$, as

$$m_{s,k}(t) = Al_k\varepsilon_{s,k}c_{s,k}(t) \tag{53}$$

Using (53), (36) and (B.5), it can be readily shown that the sum of the rate of change in the mass of the lithium ions in the solid phase is zero, that is,

$$\sum_{k\in S^+\cup S^-} \frac{dm_{s,k}(t)}{dt} = \frac{1}{F}\sum_{k\in S^+\cup S^-} C^*_{s,k}\frac{dV^*_{s,k}}{dt} = \frac{1}{F}\left(\sum_{k\in S^+} I_{\text{ionic},k} + \sum_{k\in S^-} I_{\text{ionic},k}\right) = \frac{1}{F}\left[I_{\text{app}} + (-I_{\text{app}})\right] = 0 \tag{54}$$

Hence, the mass of the lithium ions in the solid phase is conserved. On the other hand, the mass of the lithium ions in the CV k in the electrolyte is given by

$$m_{e,k}(t) = Al_k\varepsilon_{e,k}c_{e,k}(t) \tag{55}$$

Similarly, using (33) and (55), it can be readily shown that

$$\begin{aligned}\sum_{k\in S} \frac{dm_{e,k}(t)}{dt} &= \sum_{k\in S} l_k A\varepsilon_{e,k}\frac{dc_{e,k}(t)}{dt} = \frac{t^0_a}{F}\sum_{k\in S} C_{d,k}\frac{dV_{e,k}}{dt} \\ &= -\frac{t^0_a}{F}\left(\sum_{k\in S^+} I_{\text{ionic},k} + \sum_{k\in S^-} I_{\text{ionic},k}\right) = -\frac{t^0_a}{F}\left[I_{\text{app}} + (-I_{\text{app}})\right] = 0\end{aligned} \tag{56}$$

Equation (56) indicates that the mass of the lithium ions in the electrolyte is also conserved at all times. The proposed ECM establishes a relationship between charge conservation and mass conservation, as the

lithium ions are charged particles. This feature of mass conservation is a welcome benchmarking outcome for the physical credibility of the developed ECM. Its importance is also realized, for example, when it is necessary to estimate the state-of-charge of the battery where the selection of control parameters for the state estimator is constrained by mass conservation, as is reported in [42].

3.7. Equivalent circuits for thermal model

Table 3 shows that various R and C parameters are affected by the temperature T_k. As mentioned earlier, the proposed ECMs assume that the value of T_k is given. A thermal model can be incorporated to describe the heat transfer process that governs the variation of T_k in the cell. In this subsection, a technique to incorporate the thermal model to the developed ECMs is shown. The equations and the boundary conditions that describe the heat transfer phenomenon in the Li-ion cell is given as [29]

$$\rho c_p \frac{\partial T(x,t)}{\partial t} = \frac{\partial}{\partial x}\left(\lambda \frac{\partial T(x,t)}{\partial x}\right) + q_T(x,t) \tag{57}$$

$$q_T(x,t) = q_{T,\text{ohm}}(x,t) + q_{T,\text{rxn}}(x,t) + q_{T,\text{rev}}(x,t) \tag{58}$$

$$\lambda \frac{\partial T(x,t)}{\partial x}\bigg|_{x=0^+,0^-} = h(T_{\text{end}} - T(x,t))|_{x=0^+,0^-} \tag{59}$$

$$\left.\begin{aligned} q_{T,\text{ohm}}(x,t) &= \sigma\Big(\tfrac{\partial \Phi_s(x,t)}{\partial x}\Big)^2 + \kappa \tfrac{\partial \Phi_e(x,t)}{\partial x}\left(\tfrac{\partial \Phi_e(x,t)}{\partial x} + \tfrac{2RT(x,t)t_a^0}{F}\tfrac{\partial \ln c_e(x,t)}{\partial x}\right) \\ q_{T,\text{rxn}}(x,t) &= Faj(x,t)\eta_s(x,t) \\ q_{T,\text{rev}}(x,t) &= Faj(x,t)T(x,t)\tfrac{\partial U_{\text{ss}}}{\partial T}\big|_{T^*} \end{aligned}\right\} \tag{60}$$

where T_{end} is the temperature at the end of the electrode. ρ, c_p, and λ are the density, the specific heat and thermal conductivity, respectively. The heat flux q_T consists of three components: 1) the heat $q_{T,\text{ohm}}$ generated due to the movement of the electrons in the conductive pass; 2) the heat $q_{T,\text{rxn}}$ generated due to the main chemical reaction which is an exothermal reaction; 3) the heat $q_{T,\text{rev}}$ generated due to reversible entropy of reaction.

Using the FVM equations (25)–(27) to discretize (57)–(60), one obtains an equivalent thermal circuit form

$$C_{T,k}\frac{dT_k(t)}{dt} = \frac{T_{k+0.5}(t) - T_k(t)}{R_{T,k,k+0.5}} - \frac{T_k(t) - T_{k-0.5}(t)}{R_{T,k,k-0.5}} + Q_{T,k}(t) \tag{61}$$

$$Q_{T,k}(t) = l_k A q_{T,k}(t) = Q_{T,\text{ohm},k}(t) + Q_{T,\text{rxn},k}(t) + Q_{T,\text{rev},k}(t) \tag{62}$$

$$\frac{T_{k+0.5}(t) - T_k(t)}{R_{d,k,k+0.5}} = \frac{T_{\text{end}} - T_k(t)}{R_{T,\text{end}}} \tag{63}$$

$$\left.\begin{aligned} Q_{T,\text{ohm},k}(t) &= (0.5R_{s,k})(I^2_{s,k-0.5}(t) + I^2_{s,k+0.5}(t)) + (0.5R_{e,k})(I^2_{e,k-0.5}(t) + I^2_{e,k+0.5}(t)) \\ &+ I_{e,k-0.5}(t)(V_{e,k-0.5}(t) - V_{e,k}(t)) + I_{e,k+0.5}(t)(V_{e,k}(t) - V_{e,k+0.5}(t)) \\ Q_{T,\text{rxn},k}(t) &= R_{\eta,k} I^2_{\text{ionic},k}(t) \\ Q_{T,\text{rev},k}(t) &= V_{sT,k}(t) I_{\text{ionic},k}(t) \end{aligned}\right\} \tag{64}$$

where the circuit parameters are defined as

$$C_{T,k} = \rho_k c_{p,k} l_k A, \quad R_{T,k,k\pm0.5} = \frac{0.5 l_k}{\lambda_{k\pm0.5} A}, \quad R_{T,\text{end}} = \frac{1}{hA} \tag{65}$$

As shown in (62), heat flow rate $Q_{T,k}(t)$ consists of the heat rate $Q_{T,\text{ohm},k}$ due to the resistive loss in $R_{s,k}$ and $R_{e,k}$; heat rate $Q_{T,\text{rxn},k}$ due to the reactive loss in $R_{\eta,k}$ and heat rate $Q_{T,\text{rev},k}$ associated with the reversible entropy of reaction $C_{\text{sT},k}$. They can be calculated from the ODE-ECM developed in Section 3. Note in the ODE-ECM, the resistances $R_{d,k}$ and $R_{1,k}$, which are derived from the diffusion equations, do not produce any heat. They only represent the dissipative effect in the irreversible diffusion process. With the temperature T_k as additional state variables to capacitor voltages, the RC parameters are still explicit functions of the state variables, and the resulting model remains an ODE system although the system order is increased by N. The corresponding state-space representation of (61) is in the form

$$\frac{d}{dt}\mathbf{x}_T(t) = \mathbf{A}_T \mathbf{x}_T(t) + \mathbf{B}_T \mathbf{Q}_T(t) \tag{66}$$

$$\mathbf{Q}_T(t) = \mathbf{H}\mathbf{x}_c(t) + \mathbf{G}u(t) \tag{67}$$

where

$$\mathbf{x}_T(t) = \begin{bmatrix} T_1(t) & T_2(t) & \cdots & T_N(t) \end{bmatrix}^T, \ \mathbf{Q}_T(t) = \begin{bmatrix} Q_{T,1}(t) & Q_{T,2}(t) & \cdots & Q_{T,N}(t) \end{bmatrix}^T \tag{68}$$

The matrices $\mathbf{A}_T$ and $\mathbf{B}_T$, $\mathbf{H}$, and $\mathbf{G}$ can be obtained using (61) and (64), although for reason of brevity, the derivations are not given explicitly here. With the temperature state equations (66) and (67) and ODE-ECM (40), the complete state-space equation can be written as

$$\frac{d}{dt}\begin{bmatrix} \mathbf{x}_c(t) \\ \mathbf{x}_T(t) \end{bmatrix} = \begin{bmatrix} \mathbf{A}_c & \mathbf{0} \\ \mathbf{B}_T\mathbf{H} & \mathbf{A}_T \end{bmatrix} \begin{bmatrix} \mathbf{x}_c(t) \\ \mathbf{x}_T(t) \end{bmatrix} + \begin{bmatrix} \mathbf{B}_c \\ \mathbf{B}_T\mathbf{G} \end{bmatrix} u(t) \tag{69}$$

3.8. Equivalent circuits for side reactions

This subsection briefly discusses the method to incorporate the degradation model into the developed ECM. Various causes of Li-ion battery degradation have been investigated and identified, see e.g., [43, 44], based on which numerous degradation models have been developed in recent years for the behavioral prediction of Li-ion battery [5, 7, 8, 10, 45, 46]. In the present study, attention is only directed towards the most common and significant degradation mechanism encountered during the normal operations of the Li-ion battery: that due to the irreversible side reactions between the lithium ions and solvent species in the negative electrode of the battery cell. This side reactions process causes the capacity fade and the growth of SEI film in the negative electrode, and it has been widely considered in the design of ABMS [5, 43, 44].

In the P2D model presented in Table 1, the intercalation current density $J(x,t)$ in (2), (4), and (9) shall be replaced by the total local volumetric current density $J_{\text{tot}}(x,t)$. $J_{\text{tot}}(x,t)$ consists the intercalation current density $J(x,t)$ and the side reactions current density $J_{\text{sr}}(x,t)$, i.e.,

$$J_{\text{tot}}(x,t) = J(x,t) + J_{\text{sr}}(x,t) \tag{70}$$

The kinetics of the side reactions are described using the Tafel equation, by assuming the side reactions are irreversible, i.e.,

$$J_{\mathrm{sr}}(x,t) = -i_{0,\mathrm{sr}} a \exp\left(\frac{-F\eta_{\mathrm{sr}}(x,t)}{2R_g T(x,t)}\right) \tag{71}$$

$$\eta_{\mathrm{sr}}(x,t) = \Phi_s(x,t) - \Phi_e(x,t) - U_{\mathrm{sr,ref}} - \frac{J_{\mathrm{tot}}(x,t)}{a} r_f(x,t) \tag{72}$$

where $i_{0,\mathrm{sr}}$, η_{sr}, and $U_{\mathrm{sr,ref}}$ are the exchange current density, the activation overpotential, and the equilibrium potential of the side reactions, respectively.

Furthermore, the increase of SEI film resistance due to side reactions current density J_{sr} is described by

$$r_f(x,t) = -\int_0^t \frac{M_f}{\rho_f} \frac{1}{F\kappa_f a} J_{\mathrm{sr}}(x,\tau) d\tau + r_{f,0} \tag{73}$$

Here, M_f, ρ_f, κ_f, and $r_{f,0}$ are the average molecular weight, the density, the conductivity, and the initial value of the SEI film, respectively. Based on the FVM and method of electrical analogy, the equivalent circuit that represents the side reactions model (69)–(71) in an ES can be obtained. It is also shown in Fig. 3(a), in which the local side reactions current is defined as $I_{\mathrm{sr},k} = Al_k J_{\mathrm{sr},k}$. An extra equation derived from (72) shall be used to update the SEI film resistance $R_{f,k}$, i.e.,

$$R_{f,k}(t) = -\frac{1}{(Al_k a_k)^2} \frac{M_f}{\rho_f} \frac{1}{F\kappa_f} \int_0^t I_{\mathrm{sr},k}(\tau) d\tau + R_{f,0} \tag{74}$$

It should be pointed out that existing works show that the side reactions can also affect other electrochemical parameters, e.g., the volume fraction of solid active material ε_s, porosity ε_e, and the effective diffusion coefficient of electrolyte D_e, amongst others [8]. Extra equations can be added to dynamically update the associated resistances and capacitances in the ECM.

As the purpose of the current work is to provide a generic numerical methodology based on existing well-developed electrochemical models, the detailed studies on various degradation models will not be elaborated and they are left as part of future work.

4. Results and discussion

The P2D model (1)–(11) of a Li-ion battery given in Section 2.1 has been experimentally validated in various studies such as [33]. Therefore the P2D model shall be used herewith as a benchmark for validating the developed physics-based ECMs. The P2D model was implemented and solved in COMSOL Multiphysics® Modeling Software. The developed DAE-ECM and ODE-ECM were implemented in MATLAB R2016a/Simulink 8.7 software, and the variable-step solver `ode23tb` (stiff/TR-BDF2) was selected. To demonstrate the effectiveness of the proposed ECMs, the results were also compared with those obtained from a MATLAB code of P2D model named LIONSIMBA [31]. LIONSIMBA uses IDA package [47] to solve the set of DAEs with a good trade-off between accuracy and computational time based on

FVM. As LIONSIMBA and the proposed ECMs are all based on FVM, the same number of CV or ES $(N^+, N^{\text{sep}}, N^-) = (10, 5, 10)$, maximum step-size of 0.5 s, and two-parameter polynomial approximation (12) were used for consistency. All the simulated results were obtained on a 64-bit Windows 7 on a Dell OptiPlex 9020 PC, with Intel Core i7-4790 CPU@ 3.60 Hz and 16GB RAM. All the parametric values adopted for this study and the relevant references for these values are given in Appendix D.

4.1. Constant current discharge — isothermal condition

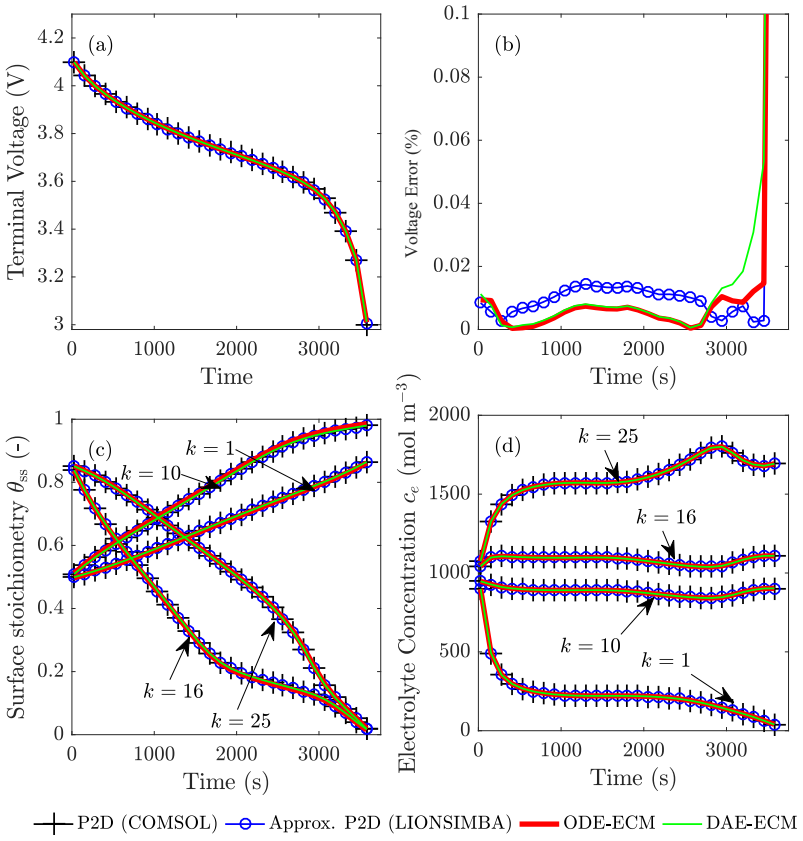

Figure 5: Simulation results under 1C discharge current from COMSOL, LIONSIMBA, ODE-ECM, and DAE-ECM. (a) Terminal voltage; (b) Voltage error compared with COMSOL results in percentage; (c) Surface stoichiometry of Li-ion in the solid phase of electrodes; (d) Li-ion concentration in the electrolyte.

Fig. 5 shows a comparison of the results from different models for a 1C constant current discharge. The simulated cells were initially fully charged at 4.17 V, and discharge was stopped at 3.0 V. In this case, a large value, $h = 1000\ \text{W} \cdot \text{m}^{-2} \cdot \text{K}^{-1}$, of the heat transfer coefficient was selected in order to simulate an isothermal condition on the left and the right external boundaries ($x = 0^{\pm}$) of the cell. The computational performance of each model and the root mean square error (RMSE) relative to the COMSOL P2D model output is given in Table 4. It can be observed in Fig. 5(a) that the outputs from the two ECMs compare very

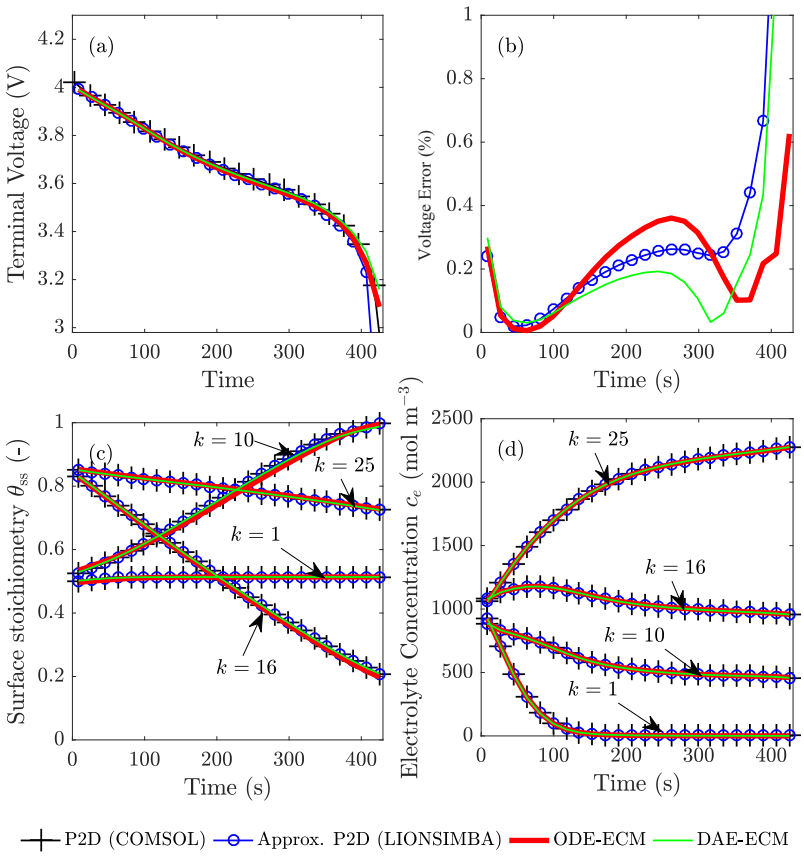

Figure 6: Simulation results under 3C discharge current from COMSOL, LIONSIMBA, ODE-ECM, and DAE-ECM. (a) Terminal voltage; (b) Voltage error compared with COMSOL results in percentage; (c) Surface stoichiometry of Li-ion in the solid phase of electrodes; (d) Li-ion concentration in the electrolyte.

favorably to that of the P2D model implementations. Indeed, the RMSE of the DAE-ECM and ODE-ECM are 0.0093% and 0.0082%, respectively, indicating that both have achieved similar accuracy under this test condition. Fig. 5(c) and Fig. 5(d) show the comparison of the Li-ion stoichiometry in the solid phase and the Li-ion concentration in the electrolyte, respectively. Again, it can be seen that the results from the two ECMs compare very well to those of the P2D implementations. It is noted that the execution time for the ODE-ECM is 1.82 s, compared to the 1.15 s for the LIONSIMBA code on the same computer. The DAE-ECM takes a significantly longer time (29.3 s) to complete the simulation than the other models.

Fig. 6 shows the same comparisons as given in Fig. 5, except for a 3C constant current discharge rate. In this instance, the RMSE for the voltage increases for each implementation. This is due to the poorer performance caused by the two-parameter approximation (12) at a higher current level. Nevertheless, the performance of ODE-ECM still compares favorably to the DAE-ECM and the P2D models, as the execution time is 1.25 s and the overall RMSE is only 0.18%.

Table 4: Comparison of different models under constant discharge current (using two-parameter parabolic approximation of solid-phase diffusion equation)

Model	1C Discharge		3C Discharge	
	Execution Time	RMSE	Execution Time	RMSE
P2D (COMSOL)	21.6 s	–	19.3 s	–
Approx. P2D (LIONSIMBA)	1.15 s	0.0143%	0.86 s	0.21%
DAE-ECM	29.3 s	0.0093%	12.38 s	0.15%
ODE-ECM	1.82 s	0.0082%	1.25 s	0.18%

The distribution of Li-ion concentration in the electrolyte is shown in Fig. 7 and Fig. 8 for the 1C and 3C discharge cases, respectively. The vertical dotted lines at $k = 10.5$ and $k = 15.5$ represent the interface between the electrodes and the separator domains. It can be seen that the boundary conditions and the continuity of the concentration are handled well by the ECMs.

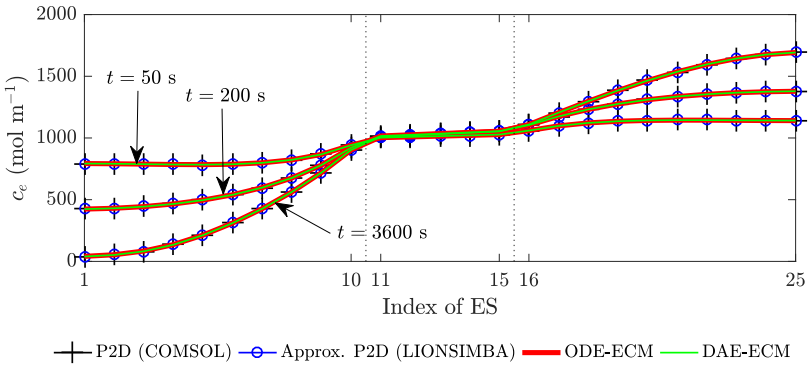

Figure 7: Simulation results under 1C discharge current: Distribution of Li-ion concentration in the electrolyte across the x-domain at three time points.

4.2. Constant current discharge — non-isothermal condition

Next, the capability of the proposed ECM to incorporate the thermal model is examined. Fig. 9(a) shows the temperature profile in time at the right end of the negative electrode ($x = 0^-$) for the same 1C discharge test in Section 4.1. However, the heat transfer coefficient was decreased to 0.01 $\mathrm{W \cdot m^{-2} \cdot K^{-1}}$, 0.1 $\mathrm{W \cdot m^{-2} \cdot K^{-1}}$, and 1 $\mathrm{W \cdot m^{-2} \cdot K^{-1}}$, respectively, to simulate three different non-isothermal conditions. Only profiles at $x = 0^-$ have been shown as it has been observed that there is very little difference in these profiles for other values of x (temperature difference between different nodes < 0.05 K). The voltage differences of the ECMs compared to that from LIONSIMBA are shown in Fig. 9(b). It can be seen that the cell temperature and voltage from the two ECMs are close to LIONSIMBA results. In this case, both

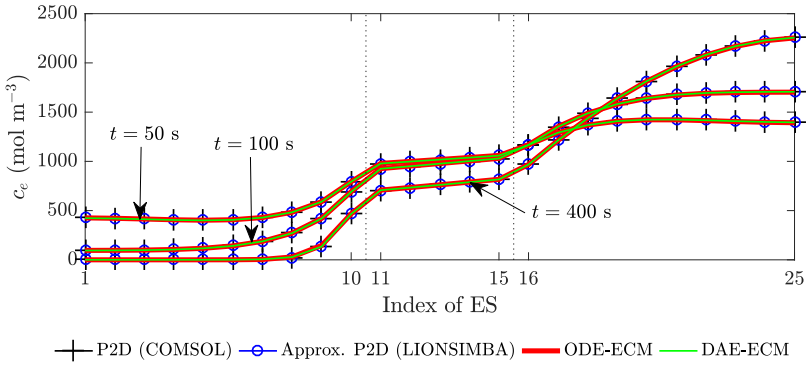

Figure 8: Simulation results under 3C discharge current: Distribution of Li-ion concentration in the electrolyte across the x-domain at three time points.

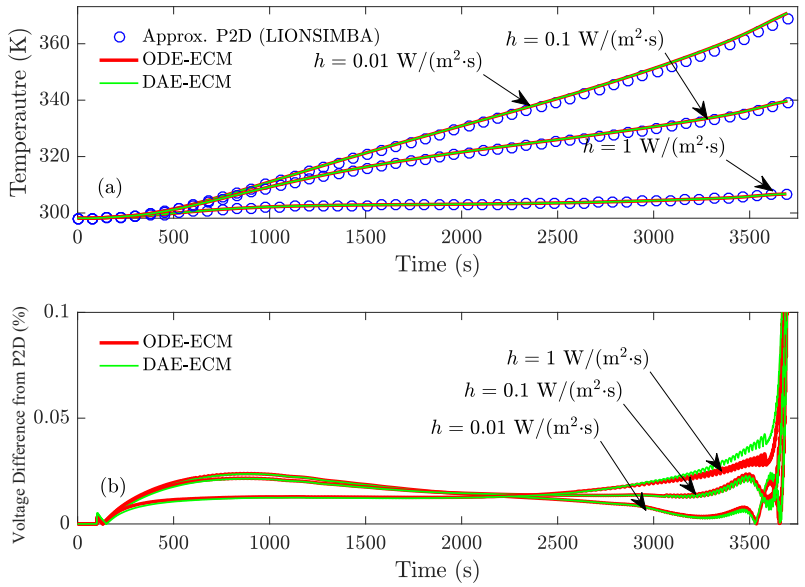

Figure 9: Comparison of simulated temperature and voltage error of 1C discharge current with different heat transfer coefficients.

ECMs accurately predict the thermal behavior of the battery. However, as noted above, the execution time of the ODE-ECM (2.3 s) is much shorter than that of the DAE-ECM (34.7 s).

4.3. Model comparison under UDDS dynamic current profile

Fig. 10 shows the comparison between ODE-ECM and LIONSIMBA P2D model under a dynamic UDDS drive cycle current profile [48]: a standard test profile adopted in many studies to evaluate the performance of batteries used in electric vehicles. Three UDDS drive cycles are concatenated, and the magnitude of the current has been doubled to create a longer and more dynamic scenario: the maximum discharge current rate is about 4.3C, and the total test period is one hour. Fig. 10 shows that the maximum voltage difference

between the two models is about 0.2% and the RMSE is less than 0.01%. The execution time using the developed ODE-ECM is about 3.7 s, while LIONSIMBA takes 942.5 s to complete the simulation. It can be seen that compared to the previous cases of constant current discharge, in which the ODE-ECM has similar performance to LIONSIMBA, but the improvement on simulation speed is significant for the ODE-ECM without the loss of accuracy. It is noted that the performance of a DAE-based ECM proposed in [24], where the execution time for a 25-min real-world load-cycle, was given as 42.57 s with the maximum voltage error of 0.2% compared to the experimental results.

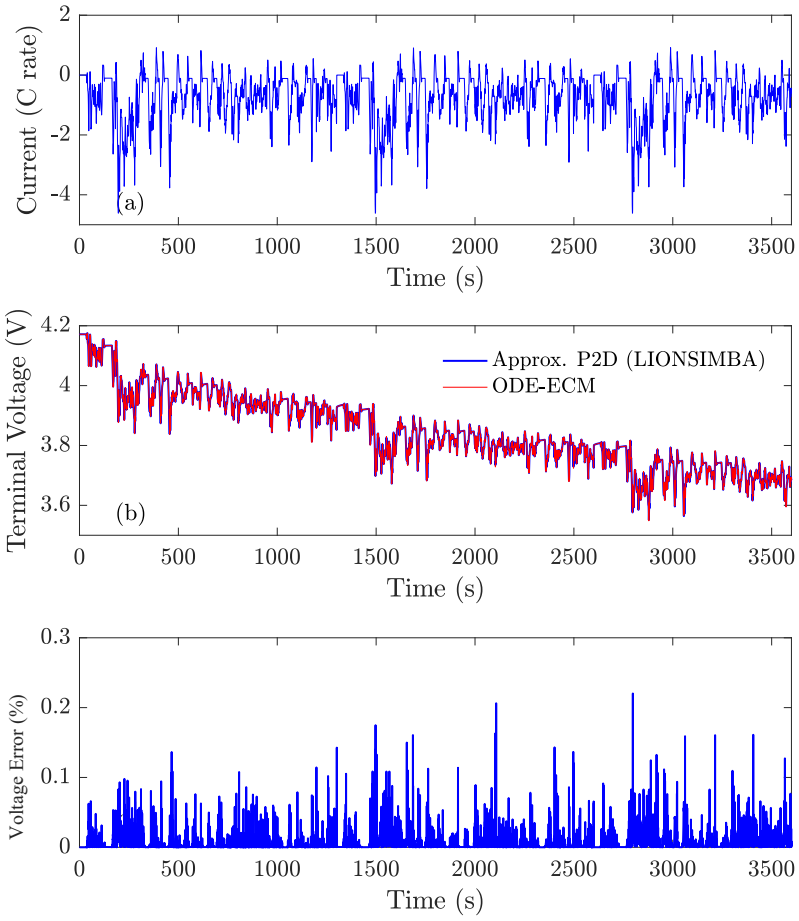

Figure 10: Simulated results under revised UDDS current profile using P2D model (LIONSIMBA) and ODE-ECM.

5. Conclusion

This paper proposes a distributed-parameter equivalent circuit model for Li-ion battery cells based on electrochemical principles using the finite volume method. Compared to the existing Li-ion cell model, the algebraic equations that require iterative solution methods have been removed, and the resulting ODE-

based system can be solved rapidly using the proposed method with high accuracy, making it superior to the existing physics-based Li-ion cell models, especially in the real-time dynamic environment, while the important features such as charge/mass and energy conservation are preserved. Other internal phenomena of the cell, such as thermal effects, can be readily incorporated into the developed ECM with low computational requirements. The model can be used in computer simulation and real-time control system design for advanced battery management schemes. As the performance of the proposed ECM also depends on the selection of the number of elementary sections and approximation methods of the solid-phase diffusion equation (6), the relevant study has been left for future work which can be expected to bring fruitful outcomes.

Appendix A.

The equations given below describe the material-dependent electrochemical characteristics of the electrode and electrolyte for $LiCoO_2$ positive electrode and LiC_6 negative electrode.

$$f_s^+(\theta_{\rm ss}^+) = \frac{-4.656 + 88.669(\theta_{\rm ss}^+)^2 - 401.119(\theta_{\rm ss}^+)^4 + 342.909(\theta_{\rm ss}^+)^6 - 462.471(\theta_{\rm ss}^+)^8 + 433.434(\theta_{\rm ss}^+)^{10}}{-1 + 18.933(\theta_{\rm ss}^+)^2 - 79.532(\theta_{\rm ss}^+)^4 + 37.311(\theta_{\rm ss}^+)^6 - 73.083(\theta_{\rm ss}^+)^8 + 95.96(\theta_{\rm ss}^+)^{10}} \tag{A.1}$$

$$\begin{aligned} f_s^-(\theta_{\rm ss}^-) = 0.7222 + 0.1387(\theta_{\rm ss}^-) + 0.029(\theta_{\rm ss}^-)^{0.5} - 0.0172(\theta_{\rm ss}^-)^{-1} + 0.0019(\theta_{\rm ss}^-)^{-1.5} + \\ 0.2808\exp(0.9 - 15\theta_{\rm ss}^-) - 0.7984\exp(0.4465\theta_{\rm ss}^- - 0.4108) \end{aligned} \tag{A.2}$$

$$f_T^+(\theta_{\rm ss}^+) = \frac{-0.001\left(0.199521039 - 0.928373822(\theta_{\rm ss}^+) + 1.364550689(\theta_{\rm ss}^+)^2 - 0.611544894(\theta_{\rm ss}^+)^3\right)}{1 - 5.661479887(\theta_{\rm ss}^+) + 11.47636191(\theta_{\rm ss}^+)^2 - 9.824312136(\theta_{\rm ss}^+)^3 + 3.048755063(\theta_{\rm ss}^+)^4} \tag{A.3}$$

$$f_T^-(\theta_{\rm ss}^-) = \frac{0.001\begin{pmatrix} 0.005269056 + 3.299265709(\theta_{\rm ss}^-) - 91.79325798(\theta_{\rm ss}^-)^2 + 1004.911008(\theta_{\rm ss}^-)^3 \\ -5812.278127(\theta_{\rm ss}^-)^4 + 19329.7549(\theta_{\rm ss}^-)^5 - 37147.8947(\theta_{\rm ss}^-)^6 + \\ 38379.18127(\theta_{\rm ss}^-)^7 - 16515.05308(\theta_{\rm ss}^-)^8 \end{pmatrix}}{\begin{pmatrix} 1 - 48.09287227(\theta_{\rm ss}^-) + 1017.234804(\theta_{\rm ss}^-)^2 - 10481.80419(\theta_{\rm ss}^-)^3 + 59431.3(\theta_{\rm ss}^-)^4 \\ -195881.6488(\theta_{\rm ss}^-)^5 + 374577.3152(\theta_{\rm ss}^-)^6 - 385821.1607(\theta_{\rm ss}^-)^7 + 165705.8597(\theta_{\rm ss}^-)^8 \end{pmatrix}} \tag{A.4}$$

$$\kappa = \varepsilon_e^{\rm brugg} \times 10^{-4} \times c_e(x,t)\begin{pmatrix} -10.5 + 0.668 \times 10^{-3} c_e(x,t) + 0.494 \times 10^{-6} c_e^2(x,t) + \\ (0.074 - 1.78 \times 10^{-5} c_e(x,t) - 8.86 \times 10^{-10} c_e^2(x,t))T(x,t) \\ +(-6.96 \times 10^{-5} + 2.8 \times 10^{-8} c_e(x,t))T^2(x,t) \end{pmatrix}^2 \tag{A.5}$$

$$D_e = \varepsilon_e^{\text{brugg}} \times 10^{-4} \times 10^{-4.43 - \frac{54}{T(x,t)-229-5.0\times10^{-3}c_e(x,t)} - 0.22\times10^{-3}c_e(x,t)} \tag{A.6}$$

$$k_0 = k_0^* \exp\left(-\frac{E_a^k}{R_g}\left(\frac{1}{T(x,t)} - \frac{1}{T^*}\right)\right) \tag{A.7}$$

$$D_s = D_s^* \exp\left(-\frac{E_a^{Ds}}{R_g}\left(\frac{1}{T(x,t)} - \frac{1}{T^*}\right)\right) \tag{A.8}$$

Appendix B.

Appendix B.1. Derivation of ECM for Li-ion diffusion in electrolyte

According to (14), the electrolyte concentration can be expressed as

$$c_e(x,t) = c_e^0 \exp\left(\frac{V_e(x,t)}{\Upsilon T(x,t)}\right) \tag{B.1}$$

Taking time derivative of (B.2) gives

$$\frac{\partial c_e(x,t)}{\partial t} \approx \frac{c_e(x,t)}{\Upsilon T(x,t)} \frac{\partial V_e(x,t)}{\partial t} \tag{B.2}$$

Similarly, taking derivative of (B.1) with respect to x yields

$$\frac{\partial c_e(x,t)}{\partial x} \approx \frac{c_e(x,t)}{\Upsilon T(x,t)} \frac{\partial V_e(x,t)}{\partial x} \tag{B.3}$$

In obtaining (B.2) and (B.3), it is assumed that the relative rates of change of temperature T with respect to time and space are both much slower than those of V_e. This is normally valid because temperature variation is a relatively slow process. Substituting (B.2), (B.3), and (2) into (5), and rearranging the resulting equation gives (16).

Appendix B.2. Derivation of ECM for Li-ion diffusion in solid phase

Define a voltage term V_s^* as a function f_s of the average stoichiometry $\theta_{s,\text{avg}} = c_{s,\text{avg}}/c_{s,\max}$, i.e.,

$$V_s^* := f_s(\theta_{s,\text{avg}}) \tag{B.4}$$

Function f_s is given in (A.1) and (A.2) for different electrodes. The time derivative of the average concentration $\theta_{s,\text{avg}}(x,t)$ can be calculated by

$$\frac{\partial c_{s,\text{avg}}(x,t)}{\partial t} = c_{s,\max}\frac{\partial \theta_{s,\text{avg}}(x,t)}{\partial t} = c_{s,\max}\frac{\partial \theta_{s,\text{avg}}}{\partial V_s^*}\frac{\partial V_s^*(x,t)}{\partial t} = \frac{c_{s,\max}}{f'_s(\theta_{s,\text{avg}})}\frac{\partial V_s^*(x,t)}{\partial t} \tag{B.5}$$

where f_s' denotes the derivative function of f_s.

Next, denote the second term of the RHS of (10) as $V_{sT}(x,t) := f_T(\theta_{\text{ss}})(T(x,t) - T^*)$, its time derivative is thus

$$\begin{aligned}\frac{\partial V_{sT}(x,t)}{\partial t} &= (T(x,t) - T^*)\frac{\partial f_T(\theta_{\text{ss}})}{\partial t} + f_T(\theta_{\text{ss}})\frac{\partial T(x,t)}{\partial t} \\ &\approx (T(x,t) - T^*)\frac{\partial f_T(\theta_{\text{s,avg}})}{\partial t} = \frac{T(x,t) - T^*}{f'_T(\theta_{\text{s,avg}})}\frac{\partial \theta_{\text{s,avg}}(x,t)}{\partial t}\end{aligned} \tag{B.6}$$

where the effect of temperature variation is again assumed negligible. Using (C.5) and (C.6) to eliminate $\partial\theta_{s,\text{avg}}(x,t)/\partial t$, one obtains the first equation of (19).

Substituting (B.5) into (12), and considering $a = 3\varepsilon_s/R_p$ and $J = Faj$, equation (18) is obtained. Similarly, if a three-parameter polynomial approximation introduced in [11] is used instead of the two-parameter approximation, (12) can be replaced by

$$\left.\begin{aligned} \tfrac{\partial c_{s,\text{avg}}(x,t)}{\partial t} &= -\tfrac{3}{R_p} j(x,t) \\ \tfrac{\partial q_{s,\text{avg}}(x,t)}{\partial t} &= -\tfrac{30 D_s}{(R_p)^2} q_{s,\text{avg}}(x,t) - \tfrac{45}{2(R_p)^2} j(x,t) \\ \tfrac{35 D_s}{R_p}[c_{\text{ss}}(x,t) - c_{s,\text{avg}}(x,t)] - 8 D_s q_{s,\text{avg}}(t) &= -j(x,t) \end{aligned}\right\} \tag{B.7}$$

With the similar procedure to obtain the ECM for two-parameter approximation, and using the FVM for spatial discretization, the ECM for the three-parameter approximation (B.7) can be derived, i.e.,

$$\left.\begin{aligned} C^*_{s,k} \tfrac{dV^*_{s,k}(t)}{dt} &= I_{\text{ionic},k}(t) \\ C_{2,k} \tfrac{dV_{2,k}(t)}{dt} &= -\tfrac{V_{2,k}(t)}{R_{2,k}} + I_{\text{ionic},k}(t) \\ U^*_{\text{ss},k}(t) &= V^*_{s,k}(t) + [V_{2,k}(t) + \tfrac{R_{1,k}}{7} I_{\text{ionic},k}(t)] \end{aligned}\right\} \tag{B.8}$$

where

$$V_{2,k}(t) \approx \frac{-8 R_p f'_s(\theta_{s,\text{avg},k})}{35 c_{s,\max,k}} q_{s,\text{avg}}(t), \quad R_{2,k} \approx \frac{6}{7} R_{1,k}, \quad C_{2,k} \approx \frac{7}{12} C_{s,k} \tag{B.9}$$

Appendix C.

Appendix C.1. Ionic flux current

For a mesh structure in the main circuit in the electrode, according to KVL and KCL, one obtains a linear system with $N^+ + N^-$ equations:

$$V_{s,k} + R_{\Sigma,k} I_{\text{ionic},k} + V_{e,k} + R_{e,k+0.5} I_{e,k+0.5} = V_{s,k+1} + R_{\Sigma,k+1} I_{\text{ionic},k+1} + V_{e,k+1} + R_{s,k+0.5} I_{s,k+0.5} \tag{C.1}$$

where

$$I_{s,k+0.5} = \begin{cases} I_{\text{app}} - \sum_{i=1}^{k} I_{\text{ionic},i}, & k \in S^+ \\ -\sum_{i=1}^{k} I_{\text{ionic},i}, & k \in S^- \end{cases}, \quad I_{e,k+0.5} = \begin{cases} \sum_{i=1}^{k} I_{\text{ionic},i} & k \in S^+ \\ I_{\text{app}} + \sum_{i=1}^{k} I_{\text{ionic},i}, & k \in S^- \end{cases} \tag{C.2}$$

Substituting (C.2) into (C.1) and then solving the resulting equation gives the expressions of $I_{\text{ionic},k}$,

$$\mathbf{I}^+_{\text{ionic}} = \mathbf{R}_1^{-1} \left[\mathbf{R}_3 I_{\text{app}} + \mathbf{E}_1(\mathbf{V}^+_s + \mathbf{V}^+_e)\right] \tag{C.3}$$

$$\mathbf{I}^-_{\text{ionic}} = -\mathbf{R}_2^{-1} \left[\mathbf{R}_4 I_{\text{app}} + \mathbf{E}_2(\mathbf{V}^-_s + \mathbf{V}^-_e)\right] \tag{C.4}$$

where

$$\mathbf{I}^+_{\text{ionic}} = \begin{bmatrix} I_{\text{ionic},1} & I_{\text{ionic},2} & \cdots & I_{\text{ionic},N^+} \end{bmatrix}^T, \quad \mathbf{I}^-_{\text{ionic}} = \begin{bmatrix} I_{\text{ionic},N^+ + N^{\text{sep}} + 1} & I_{\text{ionic},N^+ + N^{\text{sep}} + 2} & \cdots & I_{\text{ionic},N} \end{bmatrix}^T,$$

$$\mathbf{R}_1 = \begin{bmatrix} R_{\Sigma,1} + R_{\mathrm{se},1.5} & -R_{\Sigma,2} & 0 & \dots & 0 & 0 \\ R_{\mathrm{se},2.5} & R_{\Sigma,2} + R_{\mathrm{se},2.5} & -R_{\Sigma,3} & \dots & 0 & 0 \\ R_{\mathrm{se},3.5} & R_{\mathrm{se},3.5} & R_{\Sigma,3} + R_{\mathrm{se},3.5} & \dots & 0 & 0 \\ \vdots & \vdots & \vdots & \ddots & \vdots & \vdots \\ R_{\mathrm{se},N^+-0.5} & R_{\mathrm{se},N^+-0.5} & R_{\mathrm{se},N^+-0.5} & \dots & R_{\Sigma,N^+-1} + R_{\mathrm{se},N^+-0.5} & -R_{\Sigma,N^+} \\ 1 & 1 & 1 & \dots & 1 & 1 \end{bmatrix}_{(N^+ \times N^+)},$$

$$\mathbf{R}_2 = \begin{bmatrix} R_{\Sigma,N^+ + N^{\mathrm{sep}}+1} + R_{\mathrm{se},N^+ + N^{\mathrm{sep}}+1.5} & -R_{\Sigma,N^+ + N^{\mathrm{sep}}+2} & 0 & \dots & 0 & 0 \\ R_{\mathrm{se},N^+ + N^{\mathrm{sep}}+2.5} & R_{\Sigma,N^+ + N^{\mathrm{sep}}+2} + R_{\mathrm{se},N^+ + N^{\mathrm{sep}}+2.5} & -R_{\Sigma,N^+ + N^{\mathrm{sep}}+3} & \dots & 0 & 0 \\ R_{\mathrm{se},N^+ + N^{\mathrm{sep}}+3.5} & R_{\mathrm{se},N^+ + N^{\mathrm{sep}}+3.5} & R_{\Sigma,N^+ + N^{\mathrm{sep}}+3} + R_{\mathrm{se},N^+ + N^{\mathrm{sep}}+3.5} & \dots & 0 & 0 \\ \vdots & \vdots & \vdots & \ddots & \vdots & \vdots \\ R_{\mathrm{se},N-0.5} & R_{\mathrm{se},N-0.5} & R_{\mathrm{se},N-0.5} & \dots & R_{\Sigma,N-1} + R_{\mathrm{se},N-0.5} & -R_{\Sigma,N} \\ 1 & 1 & 1 & \dots & 1 & 1 \end{bmatrix}_{(N^- \times N^-)},$$

$$\mathbf{R}_3 = \begin{bmatrix} R_{s,1.5} \\ R_{s,2.5} \\ \vdots \\ R_{s,N^+-0.5} \\ 1 \end{bmatrix}_{(N^+ \times 1)}, \quad \mathbf{R}_4 = \begin{bmatrix} R_{e,N^+ + N^{\mathrm{sep}}+1.5} \\ R_{e,N^+ + N^{\mathrm{sep}}+2.5} \\ \vdots \\ R_{e,N-0.5} \\ 1 \end{bmatrix}_{(N^- \times 1)}, \quad R_{\mathrm{se},k+0.5} := R_{s,k+0.5} + R_{e,k+0.5},$$

$$\mathbf{E}_1 = \begin{bmatrix} -1 & 1 & 0 & \dots & 0 & 0 \\ 0 & -1 & 1 & \dots & 0 & 0 \\ 0 & 0 & -1 & \dots & 0 & 0 \\ \vdots & \vdots & \vdots & \ddots & \vdots & \vdots \\ 0 & 0 & 0 & \dots & -1 & 1 \\ 0 & 0 & 0 & \dots & 0 & 0 \end{bmatrix}_{(N^+ \times N^+)}, \quad \mathbf{E}_2 = \begin{bmatrix} 1 & -1 & 0 & \dots & 0 & 0 \\ 0 & 1 & -1 & \dots & 0 & 0 \\ 0 & 0 & 1 & \dots & 0 & 0 \\ \vdots & \vdots & \vdots & \ddots & \vdots & \vdots \\ 0 & 0 & 0 & \dots & 1 & -1 \\ 0 & 0 & 0 & \dots & 0 & 0 \end{bmatrix}_{(N^- \times N^-)}.$$

Appendix C.2. State equation

Rewriting (38) and (39) in state-space form yields

$$\frac{d}{dt}\begin{bmatrix}\mathbf{V}_s^+\\ \mathbf{V}_s^-\\ \mathbf{V}_e^+\\ \mathbf{V}_e^{\text{sep}}\\ \mathbf{V}_e^-\end{bmatrix}=\begin{bmatrix}\mathbf{0}&\mathbf{0}&\mathbf{0}&\mathbf{0}&\mathbf{0}\\ \mathbf{0}&\mathbf{0}&\mathbf{0}&\mathbf{0}&\mathbf{0}\\ \mathbf{0}&\mathbf{0}&\mathbf{A}_1&\mathbf{A}_2&\mathbf{0}\\ \mathbf{0}&\mathbf{0}&\mathbf{A}_3&\mathbf{A}_4&\mathbf{A}_5\\ \mathbf{0}&\mathbf{0}&\mathbf{0}&\mathbf{A}_6&\mathbf{A}_7\end{bmatrix}\begin{bmatrix}\mathbf{V}_s^+\\ \mathbf{V}_s^-\\ \mathbf{V}_e^+\\ \mathbf{V}_e^{\text{sep}}\\ \mathbf{V}_e^-\end{bmatrix}+\begin{bmatrix}\mathbf{B}_1&\mathbf{0}\\ \mathbf{0}&\mathbf{B}_2\\ \mathbf{B}_3&\mathbf{0}\\ \mathbf{0}&\mathbf{0}\\ \mathbf{0}&\mathbf{B}_4\end{bmatrix}\begin{bmatrix}\mathbf{I}_{\text{ionic}}^+\\ \mathbf{I}_{\text{ionic}}^-\end{bmatrix} \tag{C.5}$$

where

$$\begin{bmatrix}\mathbf{A}_1&\mathbf{A}_2&\mathbf{0}\\ \mathbf{A}_3&\mathbf{A}_4&\mathbf{A}_5\\ \mathbf{0}&\mathbf{A}_6&\mathbf{A}_7\end{bmatrix}=\begin{bmatrix}-F_{1,1}&F_{1,1}&0&\cdots&0&0\\ F_{1,2}&-(F_{1,2}+F_{2,2})&F_{2,2}&\cdots&0&0\\ 0&F_{2,3}&-(F_{2,3}+F_{3,3})&\cdots&0&0\\ \vdots&\vdots&\vdots&\ddots&\vdots&\vdots\\ 0&0&0&\cdots&-(F_{N-2,N-1}+F_{N-1,N-1})&F_{N-1,N-1}\\ 0&0&0&\cdots&F_{N-1,N}&-F_{N-1,N}\end{bmatrix},$$

$$F_{i,j}:=1/(R_{d,i+0.5}C_{d,j}),$$

$$\mathbf{B}_1=\text{diag}(\frac{1}{C_{s,1}},\frac{1}{C_{s,2}},\cdots,\frac{1}{C_{s,N^+}}),\mathbf{B}_2=\text{diag}(\frac{1}{C_{s,N^++N^{\text{sep}}+1}},\frac{1}{C_{s,N^++N^{\text{sep}}+2}},\cdots,\frac{1}{C_{s,N}}),$$

$$\mathbf{B}_3=\text{diag}(\frac{1}{C_{d,1}},\frac{1}{C_{d,2}},\cdots,\frac{1}{C_{d,N^+}}),\mathbf{B}_4=\text{diag}(\frac{1}{C_{d,N^++N^{\text{sep}}+1}},\frac{1}{C_{d,N^++N^{\text{sep}}+2}},\cdots,\frac{1}{C_{d,N}}).$$

Substituting (C.3) and (C.4) into (C.5), the state equation of the state-space model is obtained, i.e.,

$$\frac{d}{dt}\begin{bmatrix}\mathbf{V}_s^+\\ \mathbf{V}_s^-\\ \mathbf{V}_e^+\\ \mathbf{V}_e^{\text{sep}}\\ \mathbf{V}_e^-\end{bmatrix}=\begin{bmatrix}\mathbf{B}_1\mathbf{R}_1^{-1}\mathbf{E}_1&\mathbf{0}&\mathbf{B}_1\mathbf{R}_1^{-1}\mathbf{E}_1&\mathbf{0}&\mathbf{0}\\ \mathbf{0}&-\mathbf{B}_2\mathbf{R}_2^{-1}\mathbf{E}_2&\mathbf{0}&\mathbf{0}&-\mathbf{B}_2\mathbf{R}_2^{-1}\mathbf{E}_2\\ \mathbf{B}_3\mathbf{R}_1^{-1}\mathbf{E}_1&\mathbf{0}&\mathbf{A}_1+\mathbf{B}_3\mathbf{R}_1^{-1}\mathbf{E}_1&\mathbf{A}_2&\mathbf{0}\\ \mathbf{0}&\mathbf{0}&\mathbf{A}_3&\mathbf{A}_4&\mathbf{A}_5\\ \mathbf{0}&-\mathbf{B}_4\mathbf{R}_2^{-1}\mathbf{E}_2&\mathbf{0}&\mathbf{A}_6&\mathbf{A}_7-\mathbf{B}_4\mathbf{R}_2^{-1}\mathbf{E}_2\end{bmatrix}\begin{bmatrix}\mathbf{V}_s^+\\ \mathbf{V}_s^-\\ \mathbf{V}_e^+\\ \mathbf{V}_e^{\text{sep}}\\ \mathbf{V}_e^-\end{bmatrix}+\begin{bmatrix}\mathbf{B}_1\mathbf{R}_1^{-1}\mathbf{R}_3\\ -\mathbf{B}_2\mathbf{R}_2^{-1}\mathbf{R}_4\\ \mathbf{B}_3\mathbf{R}_1^{-1}\mathbf{R}_3\\ \mathbf{0}\\ -\mathbf{B}_4\mathbf{R}_2^{-1}\mathbf{R}_4\end{bmatrix}I_{\text{app}} \tag{C.6}$$

Appendix C.3. Output equation

According to the structure of the equivalent circuit, the terminal voltage can be expressed as

$$\begin{aligned}V_{\text{bat}}=&(V_{s,1}+V_{e,1}+R_{\Sigma,1}I_{\text{ionic},1})-(V_{s,N}+V_{e,N}+R_{\Sigma,N}I_{\text{ionic},N})+\\&\sum_{k=1}^{N-1}R_{e,k+0.5}I_{e,k+0.5}+(R_{\text{col}}^++R_{\text{col}}^-+0.5R_{s,1}+0.5R_{s,N})I_{\text{app}}\end{aligned} \tag{C.7}$$

Substituting (C.2) into (C.7) gives the output equation of the state-space model,

$$V_{\text{bat}} = \begin{bmatrix} \mathbf{K}_1\mathbf{R}_1^{-1}\mathbf{E}_1 + \mathbf{M}_1 & \mathbf{K}_2\mathbf{R}_2^{-1}\mathbf{E}_2 - \mathbf{M}_2 & \mathbf{K}_1\mathbf{R}_1^{-1}\mathbf{E}_1 + \mathbf{M}_1 & \mathbf{0} & \mathbf{K}_2\mathbf{R}_2^{-1}\mathbf{E}_2 - \mathbf{M}_2 \end{bmatrix} \times \begin{bmatrix} \mathbf{V}_s^+ & \mathbf{V}_s^- & \mathbf{V}_e^+ & \mathbf{V}_e^{\text{sep}} & \mathbf{V}_e^- \end{bmatrix}^T + (R_{\text{col}}^+ + R_{\text{col}}^- + R_{e,\text{sep}} + \mathbf{K}_1\mathbf{R}_1^{-1}\mathbf{R}_3 + \mathbf{K}_2\mathbf{R}_2^{-1}\mathbf{R}_4)I_{\text{app}} \tag{C.8}$$

where

$$\mathbf{K}_1 = \begin{bmatrix} \sum_{i=1}^{N^+} R_{e,i+0.5} + R_{\Sigma,1} & \sum_{i=2}^{N^+} R_{e,i+0.5} & \dots & R_{e,N^+-0.5} + R_{e,N^+ +0.5} & R_{e,N^+ +0.5} \end{bmatrix}$$

$$\mathbf{K}_2 = \begin{bmatrix} R_{e,N^+ +N^{\text{sep}}+0.5} & R_{e,N^+ +N^{\text{sep}}+0.5} + R_{e,N^+ +N^{\text{sep}}+1.5} & \dots & \sum_{i=N^+ +N^{\text{sep}}}^{N-2} R_{e,i+0.5} & \sum_{i=N^+ +N^{\text{sep}}}^{N-1} R_{e,i+0.5} + R_{\Sigma,N} \end{bmatrix}$$

$$\mathbf{M}_1 = \overbrace{\begin{bmatrix} 1 & 0 & 0 & \dots & 0 \end{bmatrix}}^{1\times N^+}, \quad \mathbf{M}_2 = \overbrace{\begin{bmatrix} 0 & 0 & 0 & \dots & 1 \end{bmatrix}}^{1\times N^-}, \quad R_{e,\text{sep}} = \sum_{i=N^+ +1}^{N^+ +N^{\text{sep}}-1} R_{e,i+0.5}$$

Appendix D.

The following Li-ion battery electrochemical parameters used in this paper are obtained from [33].

Table D.5: Electrochemical parameters of Li-ion battery

Sym.	Physical meaning	Unit	Parametric value		
			Pos.	Sep.	Neg.
R_p	particle radius	m	2×10^{-6}	–	2×10^{-6}
D_s^*	solid-phase diffusion coefficient	$\mathrm{m}^2 \cdot \mathrm{s}^{-1}$	1.0×10^{-14}	–	3.9×10^{-14}
a	specific surface area of electrode	m^{-1}	8.85×10^5	–	7.236×10^5
L	thickness of the electrode	m	8.0×10^{-5}	2.5×10^{-5}	8.8×10^{-5}
ε_s	volume fraction of the solid phase	–	0.59	–	0.4824
ε_e	porosity	–	0.385	0.724	0.485
σ	solid-phase conductivity	$\mathrm{S} \cdot \mathrm{m}^{-1}$	100	–	100
brugg	Bruggeman coefficient	–	4	4	4
$c_{s,\max}$	maximum concentration in solid phase	$\mathrm{mol} \cdot \mathrm{m}^{-3}$	51554	–	30555
$\theta_{0\%}$	stoichiometry for an empty battery	–	0.99174	–	0.01429
$\theta_{100\%}$	stoichiometry for a full battery	–	0.4955	–	0.8551
k^*	reaction rate constant	$\mathrm{A} \cdot \mathrm{m}^{2.5} \cdot \mathrm{mol}^{-1.5}$	2.334×10^{-11}	–	5.031×10^{-11}
ρ	density	$\mathrm{kg} \cdot \mathrm{m}^{-3}$	2500	1100	2500
λ	thermal conductivity	$\mathrm{W} \cdot \mathrm{m}^{-1} \cdot \mathrm{K}^{-1}$	2.1	0.16	1.7
c_p	specific heat	$\mathrm{J} \cdot \mathrm{kg}^{-1} \cdot \mathrm{K}^{-1}$	700	700	700
E_a^{Ds}	solid-phase diffusion activation energy	$\mathrm{J} \cdot \mathrm{mol}^{-1}$	5000	–	5000
E_a^k	reaction constant activation energy	$\mathrm{J} \cdot \mathrm{mol}^{-1}$	5000	–	5000
r_f	SEI film resistance	$\Omega \cdot \mathrm{m}^2$	0	–	0
F	Faraday constant	$\mathrm{s} \cdot \mathrm{A} \cdot \mathrm{mol}^{-1}$	96487		
T^*	reference temperature	K	298.15		
R_g	universal gas constant	$\mathrm{J} \cdot \mathrm{K}^{-1} \cdot \mathrm{mol}^{-1}$	8.314		
c_e^0	initial concentration in electrolyte	$\mathrm{mol} \cdot \mathrm{m}^{-3}$	1000		
t_a^0	transference number	–	0.636		
A	electrode plate area	m^2	1		

Nomenclature

Symbol

η	overpotential (V)
κ	electrolyte conductivity ($\mathrm{S \cdot m^{-1}}$)
λ	thermal conductivity ($\mathrm{W \cdot m^{-1} \cdot K^{-1}}$)
Φ	potential (V)
ρ	density ($\mathrm{kg \cdot m^{-3}}$)
σ	solid-phase conductivity ($\mathrm{S \cdot m^{-1}}$)
θ	stoichiometry
ε	volume fraction of a phase
A	electrode plate area ($\mathrm{m^2}$)
a	particle surface area to volume ($\mathrm{m^{-1}}$)
C	electrical capacitance (F)
c	concentration ($\mathrm{mol \cdot m^{-3}}$)
c_p	specific heat capacity ($\mathrm{J \cdot kg^{-1} \cdot K^{-1}}$)
C_T	thermal capacitance ($\mathrm{J \cdot K^{-1}}$)
D	diffusion coefficient ($\mathrm{m^2 \cdot s^{-1}}$)
F	Faraday's constant ($\mathrm{C \cdot mol^{-1}}$)
G	electrical conductance (S)
h	heat transfer coefficient ($\mathrm{W \cdot m^{-2} \cdot K^{-1}}$)
I	electric current (A)
i	electric current density ($\mathrm{A \cdot m^{-2}}$)
i_0	exchange current density ($\mathrm{A \cdot m^{-2}}$)
I_{app}	applied current (A)
i_{app}	applied charging current density ($\mathrm{A \cdot m^{-2}}$)
J	volumetric current density ($\mathrm{A \cdot m^{-3}}$)
j	pore-wall molar flux ($\mathrm{mol \cdot m^{-2} \cdot s^{-1}}$)
k_0	electrode rate constant ($\mathrm{A \cdot m^{2.5} \cdot mol^{-1.5}}$)
L	thickness of a domain (m)
l	width of a control volume (m)
M	average molecular weight ($\mathrm{kg \cdot mol^{-1}}$)
m	mass (kg)
N	number of control volume
q	concentration flux ($\mathrm{mol \cdot s^{-1}}$)
Q_T	heat transfer rate (W)
q_T	heat flux ($\mathrm{W \cdot m^{-3}}$)
R	electrical resistance (Ω)
r	areal resistance ($\mathrm{\Omega \cdot m^2}$)
R_g	universal gas constant ($\mathrm{J \cdot mol^{-1} \cdot K^{-1}}$)
R_p	particle radius (m)
R_T	thermal resistance ($\mathrm{K \cdot W^{-1}}$)
S	set
T	temperature (K)
t	time (s)
t_a^0	transference number
T_{amb}	ambient temperature (K)
U	equilibrium potential of a reaction (V)
V	voltage (V)
V_{bat}	battery terminal voltage (V)
x	macro scale index (m)

Superscript

$+$	positive electrode
$-$	negative electrode
-1	inverse

T	transpose
*	reference value at 25°
0	steady-state value
sep	separator

Subscript

d	diffusion in the electrolyte
e	electrolyte/solution phase
f	SEI film
k	central node of the the control volume k
$k+0.5$	right edge of the control volume k
$k-0.5$	left edge of the control volume k
s	solid phase
avg	average
col	current collector
max	theoretical maximum
sr	side reaction
ss	surface of solid phase

References

[1] M. T. Lawder, B. Suthar, P. W. C. Northrop, S. De, C. M. Hoff, O. Leitermann, M. L. Crow, S. Santhanagopalan, and V. R. Subramanian, "Battery energy storage system (BESS) and battery management system (BMS) for grid-scale applications," *Proc. IEEE*, vol. 102, no. 6, pp. 1014–1030, Jun. 2014.

[2] N. A. Chaturvedi, R. Klein, J. Christensen, J. Ahmed, and A. Kojic, "Algorithms for advanced battery-management systems," *IEEE Control Syst. Mag.*, vol. 30, no. 3, pp. 49–68, Jun. 2010.

[3] T. F. Fuller, M. Doyle, and J. Newman, "Simulation and optimization of the dual lithium ion insertion cell," *J. Electrochem. Soc.*, vol. 141, no. 1, pp. 1–10, 1994.

[4] M. Doyle and J. Newman, "Modeling the performance of rechargeable lithium-based cells: Design correlations for limiting cases," *J. Power Sources*, vol. 54, no. 1, pp. 46–51, Mar. 1995.

[5] P. Ramadass, B. Haran, P. M. Gomadam, R. White, and B. N. Popov, "Development of first principles capacity fade model for Li-ion cells," *J. Electrochem. Soc.*, vol. 151, no. 2, pp. A196–A203, Jan. 2004.

[6] A. V. Randall, R. D. Perkins, X. Zhang, and G. L. Plett, "Controls oriented reduced order modeling of solid-electrolyte interphase layer growth," *J. Power Sources*, vol. 209, pp. 282–288, Jul. 2012.

[7] M. B. Pinson and M. Z. Bazant, "Theory of SEI formation in rechargeable batteries: Capacity fade, accelerated aging and lifetime prediction," *J. Electrochem. Soc.*, vol. 160, no. 2, pp. A243–A250, 2013.

[8] R. Fu, S.-Y. Choe, V. Agubra, and J. Fergus, "Development of a physics-based degradation model for lithium ion polymer batteries considering side reactions," *J. Power Sources*, vol. 278, pp. 506–521, Mar. 2015.

[9] P. W. C. Northrop, B. Suthar, V. Ramadesigan, S. Santhanagopalan, R. D. Braatz, and V. R. Subramanian, "Efficient simulation and reformulation of lithium-ion battery models for enabling electric transportation," *J. Electrochem. Soc.*, vol. 161, no. 8, pp. E3149–E3157, Jan. 2014.

[10] G. Ning, R. E. White, and B. N. Popov, "A generalized cycle life model of rechargeable Li-ion batteries," *Electrochim. Acta*, vol. 51, no. 10, pp. 2012–2022, Feb. 2006.

[11] V. R. Subramanian, V. D. Diwakar, and D. Tapriyal, "Efficient macro-micro scale coupled modeling of batteries," *J. Electrochem. Soc.*, vol. 152, no. 10, pp. A2002–A2008, Aug. 2005.

[12] K. A. Smith, C. D. Rahn, and C.-Y. Wang, "Control oriented 1D electrochemical model of lithium ion battery," *Energy Convers. Manage.*, vol. 48, no. 9, pp. 2565–2578, Sep. 2007.

[13] ——, "Model-based electrochemical estimation and constraint management for pulse operation of lithium ion batteries," *IEEE Trans. Control Syst. Technol.*, vol. 18, no. 3, pp. 654–663, May 2010.

[14] T.-S. Dao, C. P. Vyasarayani, and J. McPhee, "Simplification and order reduction of lithium-ion battery model based on porous-electrode theory," *J. Power Sources*, vol. 198, pp. 329–337, Jan. 2012.

[15] M. Guo, G. Sikha, and R. E. White, "Single-particle model for a lithium-ion cell: Thermal behavior," *J. Electrochem. Soc.*, vol. 158, no. 2, pp. A122–A132, 2011.

[16] G. Ning and B. N. Popov, "Cycle life modeling of lithium-ion batteries," *J. Electrochem. Soc.*, vol. 151, no. 10, pp. A1584–A1591, 2004.

[17] D. Zhang, B. N. Popov, and R. E. White, "Modeling lithium intercalation of a single spinel particle under potentiodynamic control," *J. Electrochem. Soc.*, vol. 147, no. 3, pp. 831–838, Mar. 2000.

[18] V. Ramadesigan, P. W. C. Northrop, S. De, S. Santhanagopalan, R. D. Braatz, and V. R. Subramanian, "Modeling and simulation of lithium-ion batteries from a systems engineering perspective," *J. Electrochem. Soc.*, vol. 159, no. 3, pp. R31–R45, Jan. 2012.

[19] X. Hu, S. Li, and H. Peng, "A comparative study of equivalent circuit models for Li-ion batteries," *J. Power Sources*, vol. 198, pp. 359–367, Jan. 2012.

[20] C. Zou, C. Manzie, and D. Nesic, "A framework for simplification of PDE-based lithium-ion battery models," *IEEE Trans. Control Syst. Technol.*, vol. 24, no. 5, pp. 1594–1609, Sep. 2016.

[21] G. K. Prasad and C. D. Rahn, "Development of a first principles equivalent circuit model for a lithium ion battery," in *Proc. ASME Annu. Dyn. Syst. Control Conf. – JSME Motion Vibration Conf.* Fort Lauderdale, FL, USA: ASME, 17-19 Oct. 2012, pp. 369–375.

[22] Y. Li, D. M. Vilathgamuwa, T. W. Farrell, S. S. Choi, and N. T. Tran, "An equivalent circuit model of Li-ion battery based on electrochemical principles used in grid-connected energy storage applications," in *Proc. Int. Future Energy Electron. Conf. ECCE Asia (IFEEC 2017 - ECCE Asia).* Kaohsiung, Taiwan: IEEE, 3-7 Jun. 2017, pp. 959–964.

[23] S. Räel and M. Hinaje, "Using electrical analogy to describe mass and charge transport in lithium-ion batteries," *J. Power Sources*, vol. 222, pp. 112–122, Jan. 2013.

[24] M.-T. von Srbik, M. Marinescu, R. F. Martinez-Botas, and G. J. Offer, "A physically meaningful equivalent circuit network model of a lithium-ion battery accounting for local electrochemical and thermal behaviour, variable double layer capacitance and degradation," *J. Power Sources*, vol. 325, pp. 171–184, Sep. 2016.

[25] Y. Merla, B. Wu, V. Yufit, R. F. Martinez-Botas, and G. J. Offer, "An easy-to-parameterise physics-informed battery model and its application towards lithium-ion battery cell design, diagnosis, and degradation," *J. Power Sources*, vol. 384, pp. 66–79, Apr. 2018.

[26] P. Rabinowitz, *Numerical Methods for Nonlinear Algebraic Equations.* New York: Gordon and Breach Science Publishers, 1970.

[27] I. Mayergoyz and W. Lawson, *Basic Electric Circuit Theory: A One-semester Text.* Academic Press, 1997.

[28] W. F. Tinney and J. W. Walker, "Direct solutions of sparse network equations by optimally ordered triangular factorization," *Proc. IEEE*, vol. 55, no. 11, pp. 1801–1809, 1967.

[29] K. Kumaresan, G. Sikha, and R. E. White, "Thermal model for a Li-ion cell," *J. Electrochem. Soc.*, vol. 155, no. 2, pp. A164–A171, Feb. 2008.

[30] K. Smith and C.-Y. Wang, "Solid-state diffusion limitations on pulse operation of a lithium ion cell for hybrid electric vehicles," *J. Power Sources*, vol. 161, no. 1, pp. 628–639, Oct. 2006.

[31] M. Torchio, L. Magni, R. B. Gopaluni, R. D. Braatz, and D. M. Raimondo, "Lionsimba: A matlab framework based on a finite volume model suitable for Li-ion battery design, simulation, and control," *J. Electrochem. Soc.*, vol. 163, no. 7, pp. A1192–A1205, Jan. 2016.

[32] M. Doyle, T. F. Fuller, and J. Newman, "Modeling of galvanostatic charge and discharge of the lithium/polymer/insertion cell," *J. Electrochem. Soc.*, vol. 140, no. 6, pp. 1526–1533, Jan. 1993.

[33] P. W. C. Northrop, V. Ramadesigan, S. De, and V. R. Subramanian, "Coordinate transformation, orthogonal collocation, model reformulation and simulation of electrochemical-thermal behavior of lithium-ion battery stacks," *J. Electrochem. Soc.*, vol. 158, no. 12, pp. A1461–A1477, Jan. 2011.

[34] B. L. Trembacki, A. N. Mistry, D. R. Noble, M. E. Ferraro, P. P. Mukherjee, and S. A. Roberts, "Mesoscale analysis of conductive binder domain morphology in lithium-ion battery electrodes," *J. Electrochem. Soc.*, vol. 165, no. 13, pp. E725–E736, Jan. 2018.

[35] B. L. Trembacki, D. R. Noble, V. E. Brunini, M. E. Ferraro, and S. A. Roberts, "Mesoscale effective property simulations incorporating conductive binder," *J. Electrochem. Soc.*, vol. 164, no. 11, pp. E3613–E3626, Jan. 2017.

[36] D.-W. Chung, P. R. Shearing, N. P. Brandon, S. J. Harris, and R. E. García, "Particle size polydispersity in Li-ion batteries," *J. Electrochem. Soc.*, vol. 161, no. 3, pp. A422–A430, Jan. 2014.

[37] Q. Zhang and R. E. White, "Comparison of approximate solution methods for the solid phase diffusion equation in a porous electrode model," *J. Power Sources*, vol. 165, no. 2, pp. 880–886, Mar. 2007.

[38] Y. Zeng, P. Albertus, R. Klein, N. Chaturvedi, A. Kojic, M. Z. Bazant, and J. Christensen, "Efficient conservative numerical schemes for 1D nonlinear spherical diffusion equations with applications in battery modeling," *J. Electrochem. Soc.*, vol. 160, no. 9, pp. A1565–A1571, Jan. 2013.

[39] W. Schiesser, *The Numerical Method of Lines: Integration of Partial Differential Equations*. Academic Press, 1991.

[40] MathWorks, *Simulink User's Guide*, Mar. 2015.

[41] P. Kemper and D. Kum, "Extended single particle model of Li-ion batteries towards high current applications," in *Proc. IEEE Veh. Power Propul. Conf.*, 15-18 Oct. 2013, pp. 1–6.

[42] R. Klein, N. A. Chaturvedi, J. Christensen, J. Ahmed, R. Findeisen, and A. Kojic, "Electrochemical model based observer design for a lithium-ion battery," *IEEE Trans. Control Syst. Technol.*, vol. 21, no. 2, pp. 289–301, Jan. 2011.

[43] C. R. Birkl, M. R. Roberts, E. McTurk, P. G. Bruce, and D. A. Howey, "Degradation diagnostics for lithium ion cells," *J. Power Sources*, vol. 341, pp. 1–35, Feb. 2016.

[44] X. Feng, J. Sun, M. Ouyang, X. He, L. Lu, X. Han, M. Fang, and H. Peng, "Characterization of large format lithium ion battery exposed to extremely high temperature," *J. Power Sources*, vol. 272, pp. 457–467, Dec. 2014.

[45] J. Wang, P. Liu, J. Hicks-Garner, E. Sherman, S. Soukiazian, M. Verbrugge, H. Tataria, J. Musser, and P. Finamore, "Cycle-life model for graphite-$LiFePO_4$ cells," *J. Power Sources*, vol. 196, no. 8, pp. 3942–3948, Apr. 2011.

[46] G. L. Plett, "Algebraic solution for modeling SEI layer growth," *ECS Electrochem. Lett.*, vol. 2, no. 7, pp. A63–A65, 2013.

[47] A. C. Hindmarsh, P. N. Brown, K. E. Grant, S. L. Lee, R. Serban, D. E. Shumaker, and C. S. Woodward, "SUNDIALS: Suite of nonlinear and differential/algebraic equation solvers," *ACM Trans. Math. Softw.*, vol. 31, no. 3, pp. 363–396, 2005.

[48] S. J. Moura, J. L. Stein, and H. K. Fathy, "Battery-health conscious power management in plug-in hybrid electric vehicles via electrochemical modeling and stochastic control," *IEEE Trans. Control Syst. Technol.*, vol. 21, no. 3, pp. 679–694, May 2013.